

SANDIA REPORT

SAND87-0501 • UC-60
Unlimited Release
Printed April 1987

65598

C.1

VAWT Stochastic Wind Simulator



8232-2//065598



00000001 -

James H. Strickland

Prepared by
Sandia National Laboratories
Albuquerque, New Mexico 87185 and Livermore, California 94550
for the United States Department of Energy
under Contract DE-AC04-76DP00789

Issued by Sandia National Laboratories, operated for the United States Department of Energy by Sandia Corporation.

NOTICE: This report was prepared as an account of work sponsored by an agency of the United States Government. Neither the United States Government nor any agency thereof, nor any of their employees, nor any of their contractors, subcontractors, or their employees, makes any warranty, express or implied, or assumes any legal liability or responsibility for the accuracy, completeness, or usefulness of any information, apparatus, product, or process disclosed, or represents that its use would not infringe privately owned rights. Reference herein to any specific commercial product, process, or service by trade name, trademark, manufacturer, or otherwise, does not necessarily constitute or imply its endorsement, recommendation, or favoring by the United States Government, any agency thereof or any of their contractors or subcontractors. The views and opinions expressed herein do not necessarily state or reflect those of the United States Government, any agency thereof or any of their contractors or subcontractors.

Printed in the United States of America
Available from
National Technical Information Service
U.S. Department of Commerce
5285 Port Royal Road
Springfield, VA 22161

NTIS price codes
Printed copy: A04
Microfiche copy: A01

SAND87-0501
Unlimited Release UC-60
Printed April 14, 1987

VAWT Stochastic Wind Simulator

James H. Strickland
Sandia National Laboratories
Albuquerque, NM 87185

Abstract

A stochastic wind simulation for VAWTs (VSTOC) has been developed which yields turbulent wind-velocity fluctuations for rotationally sampled points. This allows three-component wind-velocity fluctuations to be simulated at specified nodal points on the wind-turbine rotor. A first-order convection scheme is used which accounts for the decrease in streamwise velocity as the flow passes through the wind-turbine rotor. The VSTOC simulation is independent of the particular analytical technique used to predict the aerodynamic and performance characteristics of the turbine. The VSTOC subroutine may be used simply as a subroutine in a particular VAWT prediction code or it may be used as a subroutine in an independent processor. The independent processor is used to interact with a version of the VAWT prediction code which is segmented into deterministic and stochastic modules. Using VSTOC in this fashion is very efficient with regard to decreasing computer time for the overall calculation process.

(this page intentionally left blank)

Contents

1	INTRODUCTION	1
2	GENERAL VSTOC METHODOLOGY	2
2.1	VAWT Flow Field Characteristics	2
2.2	Interfacing To VAWT Prediction Codes	4
3	WIND SIMULATION	6
3.1	Spectral Model	6
3.2	Non-dimensional Time-Series	7
3.3	Time-Series At Moving Nodes	9
4	VSTOC SUBROUTINE	13
4.1	Subroutine Description	13
4.2	Input-Output	15
5	SUMMARY AND CONCLUSIONS	18
6	REFERENCES	19
7	PROGRAM LISTING	20
7.1	VSTOC Subroutine	20
7.2	VSTOC With Input-Output Drivers	23

(This page intentionally left blank.)

1 INTRODUCTION

During the period 1973-1983, major advances were made concerning the understanding of the aerodynamic behavior of vertical-axis wind turbines (VAWTs). A review of aerodynamic analysis techniques, which were developed during that time period, is given by Strickland [1]. Prior to about 1983, virtually no attempts were made to examine the effects of atmospheric turbulence on the performance of VAWTs. This was partially due to the fact that the power output from VAWTs is not significantly affected by atmospheric turbulence. For example, in a 1981 study by Sheldahl [2], good agreement between field and wind tunnel data concerning power output were obtained. The emphasis during this time period was oriented toward the optimization of VAWTs from an energy performance standpoint. The effect of atmospheric turbulence on VAWTs became important only as designers became concerned about the structural fatigue life of such machines.

Veers [3] was one of the first investigators to examine the effects of atmospheric turbulence on VAWTs. In his work, Veers formulated a three-dimensional turbulence model for the VAWT. He then utilized a simplified version of the model in which numerous planes of coherent turbulence were first produced upstream of the turbine rotor and then convected downstream through the rotor. The convection velocity was predicted using results from a "multiple streamtube" VAWT prediction code [4]. The stochastic wind model and the aerodynamic prediction code were integrated into a single code in this study. The resulting computer code was therefore not immediately adaptable to use with other VAWT prediction codes.

In a 1984 study, George [5] obtained turbulence data for VAWTs by monitoring an array of wind sensors placed in a circle at a constant elevation. The data from these sensors were rearranged to simulate a rotational sampling sequence. Powell and Connell [6] developed a computer model for simulating turbulence data for VAWTs which is an analytical counterpart to the experimental work of George. In this work, they note that one of the effects of rotational sampling is that energy is transferred from frequencies lower than the rotational frequency to the rotational frequency and its harmonics. The major weakness of their simulation is that the effect of the wind turbine rotor on turbulence convection velocities is neglected. As will be demonstrated later, the retardation of the flow, due to the presence of the rotor, increases the transfer of energy into the rotational frequency band from lower frequencies. Therefore, it appears to be necessary to include this effect in order to obtain a valid simulation.

In the present work, the general philosophy was to provide a simulation which includes information on convective velocities through the rotor but which is not explicitly part of any particular VAWT aerodynamic code. This was accomplished by first noting the characteristics of the flow field through a VAWT. Characteristics of the streamwise convective velocity through the rotor were then placed in a model which requires only a single input parameter from a VAWT aerodynamic code.

2 GENERAL VSTOC METHODOLOGY

2.1 VAWT Flow Field Characteristics

In order to develop the VAWT STOChastic wind simulation, the nature of the flow field around a vertical-axis wind turbine was examined utilizing information obtained by Strickland and Goldman [7]. Strickland and Goldman calculated the flow field around a typical two-bladed three-dimensional vertical-axis wind turbine using a computer code based on vortex theory. A sample of these results is reproduced in Figure 1.

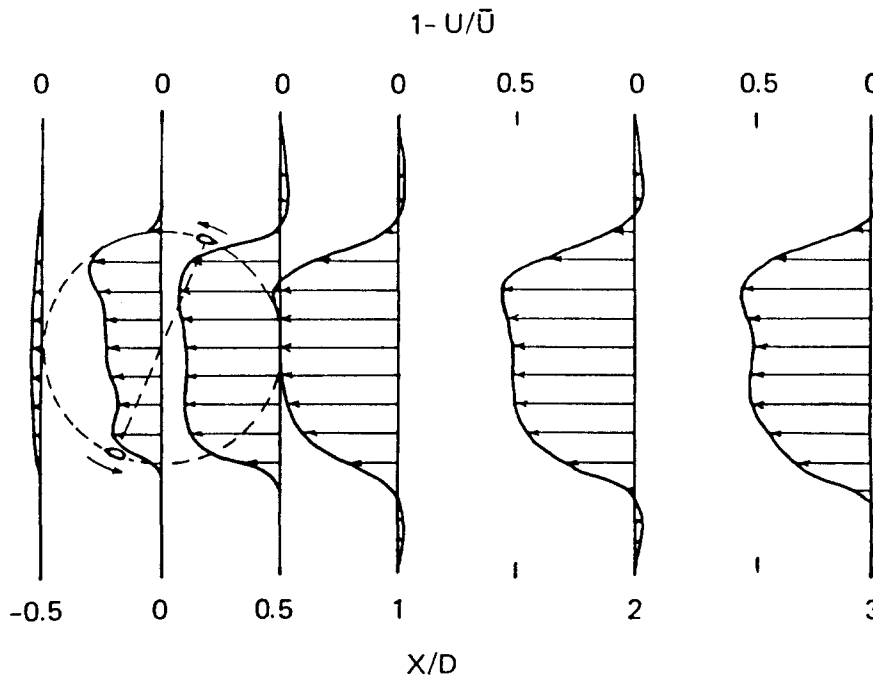


Figure 1: Calculated velocity-defect profiles for a three-dimensional two-bladed rotor.

In Figure 1, the velocity defect profiles are shown for several streamwise stations in the equatorial plane. Here \bar{U} is the upstream velocity, U is the local velocity, x is the streamwise location, and D is the wind turbine rotor diameter. Details concerning turbine operating conditions can be found in reference [7]. As can be seen in this figure, the velocity across the rotor is somewhat uniform and probably accounts for the ability of the original single-streamtube momentum model due to Templin [8] to make reasonable performance predictions. Calculated centerline velocities from [7] are shown in Figure 2. As can be seen from this figure, the centerline velocity at the upstream edge of the rotor is essentially that of the freestream. The velocity defect then varies in an approximately linear fashion through the rotor. The velocity at the downstream edge of the rotor is reasonably close to the asymptotic value of the velocity downstream of the rotor.

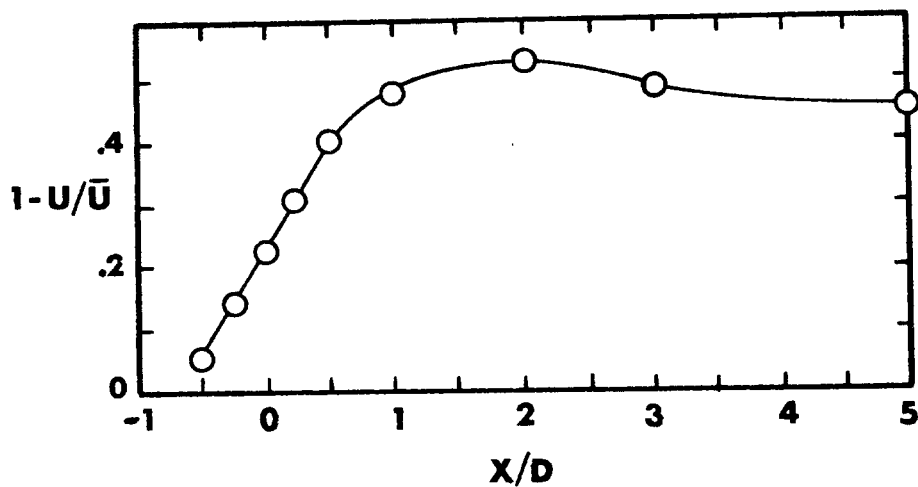


Figure 2: Centerline velocity in the near wake of a three-dimensional two-bladed rotor.

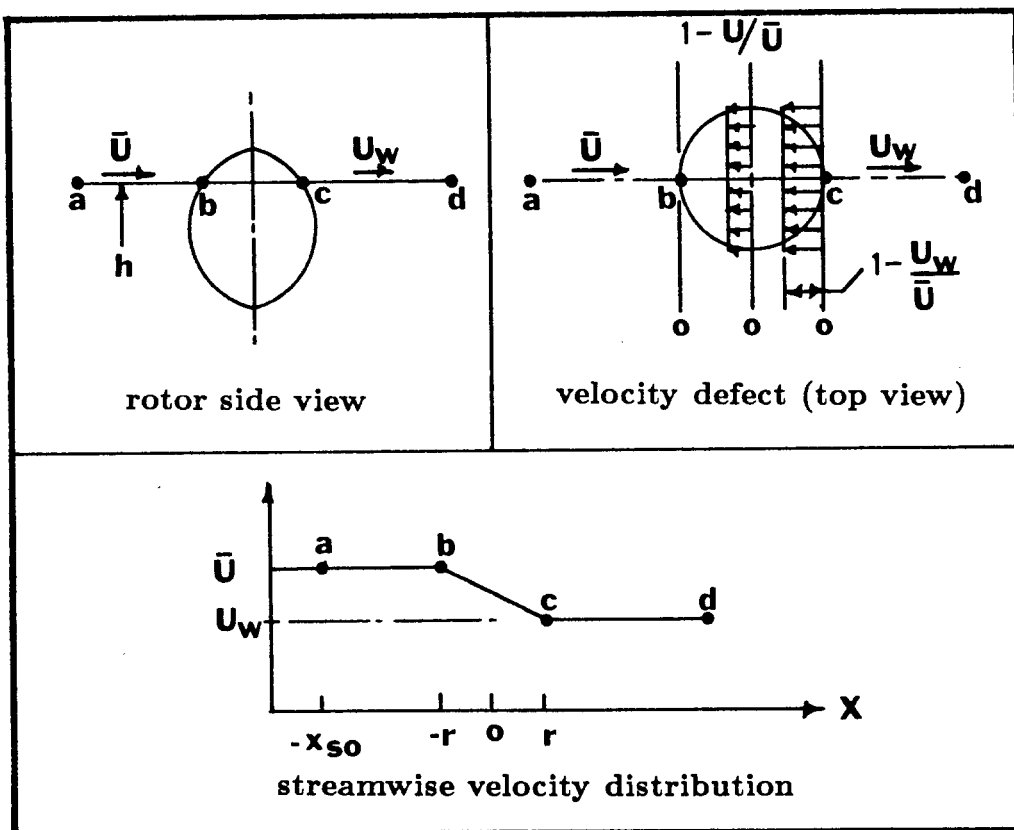


Figure 3: VSTOC velocity distribution model.

In order to model the convective velocities through the rotor, it will be assumed that the velocity profiles can be approximated as shown in Figure 3. In this figure, the convection of stochastic wind fluctuations is modeled by assuming a uniform velocity defect across the rotor with a linear variation through the rotor in the streamwise direction. The retardation of the flow begins at the position of the upstream blade passage (in that plane) and reaches the wake velocity at the position of the downstream blade passage. This simple model requires only a single input parameter (the wake velocity U_W) from the aerodynamic code. The wake velocity is the asymptotic value of the velocity in the near wake. For example, in a simple momentum model, the wake velocity defect is twice the "disk velocity" defect. In a double-multiple streamtube model, the wake velocity defect is twice the average velocity defect between the upstream and downstream rotor blade positions. For free vortex models, the wake velocity can be obtained by time averaging the velocity at the downstream edge of the rotor over one revolution.

2.2 Interfacing To VAWT Prediction Codes

The purpose of the VSTOC simulation is to provide a necessary part of a larger simulation which will produce blade load distributions as a function of time. There are essentially three parts to the overall simulation. These parts consist of a VAWT "aerodynamic module," the VSTOC module and, a VAWT "performance module." This requires that the typical VAWT prediction code be broken up into an aerodynamic module and a performance module. In general, the aerodynamic module is used to predict the deterministic fluid kinematics of the flow around the turbine, VSTOC predicts the stochastic fluid kinematics, and the performance module is used to calculate rotor blade force distributions as a function of time.

The required output from the aerodynamic module consists of velocity defect or velocity perturbation values (u_a, v_a, w_a) in the (x, y, z) directions as a function of the streamwise, vertical, and lateral position of a rotor blade element. These calculated data are required for only one revolution of the rotor since they are deterministic and periodic with time. The wake velocity U_W is also to be calculated for use in VSTOC. In the simplest case, only a single value of U_W at some reference height is required. If a non-uniform vertical distribution of U_W is desired, then such a distribution must be produced by the aerodynamic module. As mentioned previously, the aerodynamic module produces results that are deterministic. It is assumed that the wind fluctuations do not significantly affect the average periodic perturbation velocities produced by the wind machine. This assumption is completely valid for cases where the rotor blades are not experiencing aerodynamic stall (high tip-to-wind speed ratios). On the other hand, for low tip-to-wind speed ratios, where aerodynamic stall does occur, the perturbation velocities are small in comparison to the freestream velocity. Therefore, this assumption should yield good results throughout the complete operating range of tip-to-wind speed ratios. The ability to use such deterministic solutions as part of the overall calculation procedure greatly reduces computer time requirements since there is no need to make

perturbation velocity calculations for a large number of rotor revolutions. CPU time requirements would otherwise be prohibitive for VAWT aerodynamic simulations which are produced by vortex codes such as VDART3 [9].

The VSTOC simulation produces the stochastic wind perturbation velocities u' , v' , and w' for specified nodes on the rotor blade. A time-series is thus produced at each specified node. The length of the time-series is somewhat a matter of choice. In general, for good simulations, it has a duration of between 30 and 150 rotor revolutions which results in a 1,000 to 5,000 point time-series. The time increment is typically chosen to be the same as that used in the VAWT aerodynamic module.

The VAWT performance module uses the perturbation velocities (u_a, v_a, w_a) and (u', v', w') calculated by the VAWT aerodynamic module and VSTOC simulation, respectively, as input. These perturbation velocities are mixed to yield total perturbation velocities due to the presence of the rotor and due to atmospheric turbulence. Blade load calculations are then easily made based on the total perturbation velocity, the freestream velocity, and the rotor blade motion. These calculations are made for a record length which is the same as that of the VSTOC simulation. Calculations proceed rapidly in this module since the perturbation velocities are known apriori.

3 WIND SIMULATION

3.1 Spectral Model

The spectral model used in the present work is that given by Frost, Long, and Turner [10]. The spectral power density ϕ_w is given by:

$$\phi_w = \left(\frac{\sigma^2}{n}\right) \frac{0.164\eta^+/\eta_0}{1 + 0.164(\eta^+/\eta_0)^{\frac{5}{3}}} \quad (1)$$

where σ is the turbulence intensity, n is the frequency in Hz, and η^+ is the frequency normalized by the height above ground h and the mean velocity \bar{U} at that point ($\eta^+ = nh/\bar{U}$). η_0 is a constant which depends upon the x, y, z fluctuation directions ($\eta_0 = .0144, .0962, .0265$). Here x is the streamwise direction, y is the vertical direction, and z is the lateral direction.

Equation 1 does not exactly satisfy the relationship between the turbulence intensity level and the spectral power density which is given by:

$$\sigma^2 \equiv \int_0^\infty \phi_w dn. \quad (2)$$

In order to force this identity to hold, the constant in the numerator in Equation 1 was changed from 0.164 to 0.171. The actual value of the *rms* turbulence intensity is given by:

$$\sigma = \frac{\bar{U}C}{\ln\left(\frac{h}{h_0} + 1\right)} \quad (3)$$

where C is a constant which depends upon the x, y, z fluctuation directions ($C = 1.00, 0.52, 0.64$) and h_0 is the turbulence roughness height.

Finally, the spectral power density can be non-dimensionalized by normalizing with the height above ground, the mean velocity, and the turbulence intensity:

$$F \equiv \frac{\phi_w \bar{U}}{h\sigma^2} = \frac{0.171/\eta_0}{1 + 0.164(\eta^+/\eta_0)^{\frac{5}{3}}}. \quad (4)$$

At this point it is appropriate to estimate the maximum frequency which should appear in the truncated Fourier time-series used to simulate the wind perturbations. As can be seen from Equation 4, the maximum spectral contribution occurs at a zero frequency and decays asymptotically to zero for large frequencies. If one places the cut-off frequency at that value where F is 0.05 percent of its zero frequency value, then the non-dimensional cutoff frequency is :

$$\eta_{maz}^+ \simeq 283\eta_0. \quad (5)$$

Using the maximum value of η_0 one finds that η_{maz}^+ is equal to 27. For later convenience, the value of η_{maz}^+ will be set equal to 25 instead of 27.

3.2 Non-dimensional Time-Series

Using the power spectra presented in the above section one can construct a Fourier time-series representation of the fluctuation velocity. In non-dimensional form, this series can be written as:

$$V^+ = \sigma^+ \sum_{j=1}^{N_P/2} [A_j^+ \sin(2\pi\eta_j^+ \tau^+) + B_j^+ \cos(2\pi\eta_j^+ \tau^+)] \quad (6)$$

where the fluctuation velocity ($V' = u', v', \text{ or } w'$) and the *rms* turbulence intensity ($\sigma = \sigma_x, \sigma_y, \text{ or } \sigma_z$) are normalized by \bar{U} such that:

$$\begin{aligned} V^+ &= \frac{V'}{\bar{U}} \\ \sigma^+ &= \frac{\sigma}{\bar{U}}. \end{aligned} \quad (7)$$

Values for the coefficients A_j^+ and B_j^+ are given in terms of the non-dimensional spectral power density, the dimensionless frequency band $\Delta\eta^+$, and a random phase angle ϕ_j as:

$$\begin{aligned} A_j^+ &= (2F_j \Delta\eta^+)^{\frac{1}{2}} \sin \phi_j \\ B_j^+ &= (2F_j \Delta\eta^+)^{\frac{1}{2}} \cos \phi_j. \end{aligned} \quad (8)$$

The time τ is non-dimensionalized by the mean velocity and the height above ground ($\tau^+ = \tau\bar{U}/h$). The summation in Equation 6 is to be carried out for $j = 1$ to $N_P/2$, where N_P is the number of points in the time-series. The length of the time-series is related to the smallest frequency represented in the spectra by:

$$\tau_{max}^+ = \frac{1}{\Delta\eta^+}. \quad (9)$$

Since the maximum frequency is given by:

$$\eta_{max}^+ = \frac{N_P}{2} \Delta\eta^+ = 25 \quad (10)$$

then it follows that $N_P = 50\tau_{max}^+$ and $\Delta\tau^+ = 0.02$.

A typical time-series is shown in Figure 4 where N_P is equal to 1000. It is important to note that N_P should not be allowed to drop much below 1000 in order to adequately capture the low-frequency portion of the spectra. In Figure 5 the effect of N_P on the *rms* turbulence intensity as simulated by the time-series is clearly shown. In this figure, the *rms* turbulence intensity specified in the input spectra is equal to unity in all cases. This also implies that the time-series length (τ_{max}^+) should be greater than about 20.

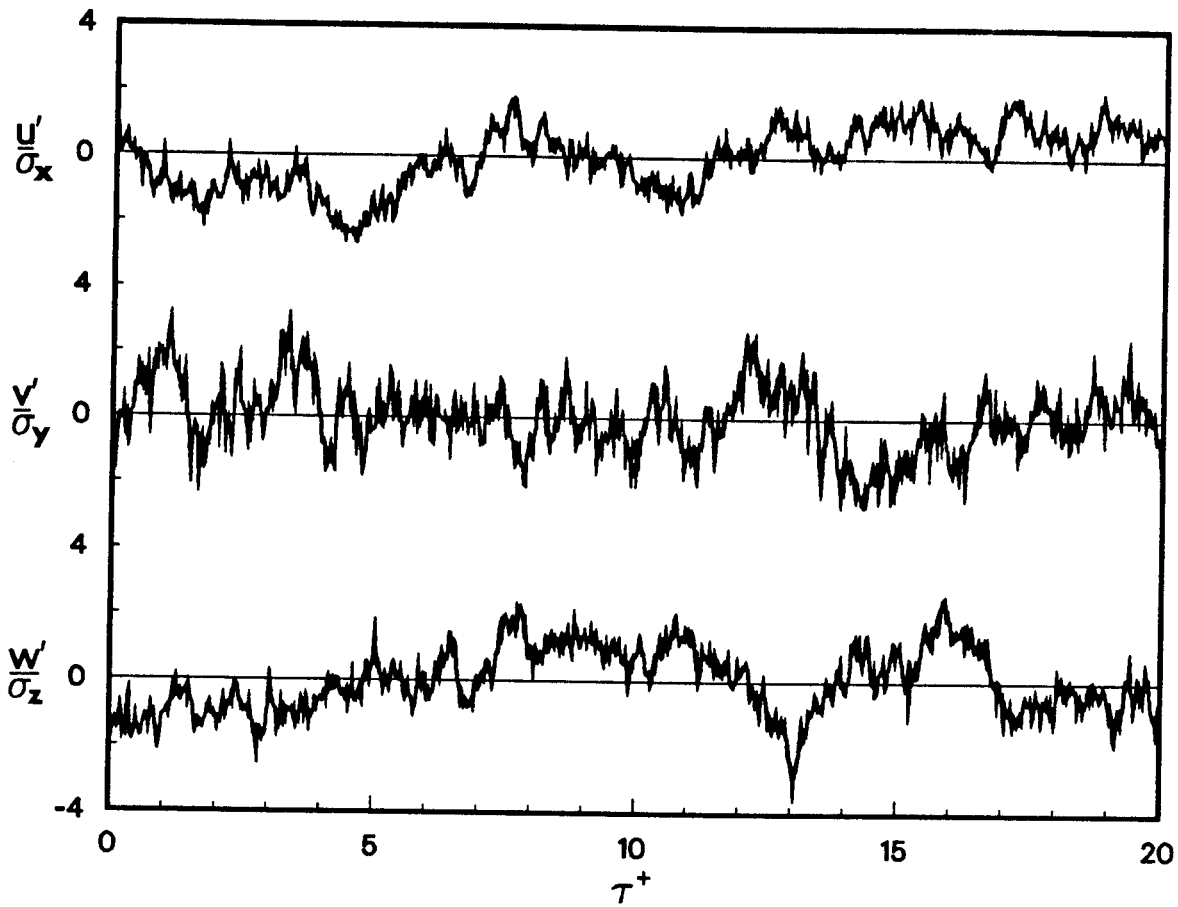


Figure 4: Time-series simulation of wind-velocity fluctuations.

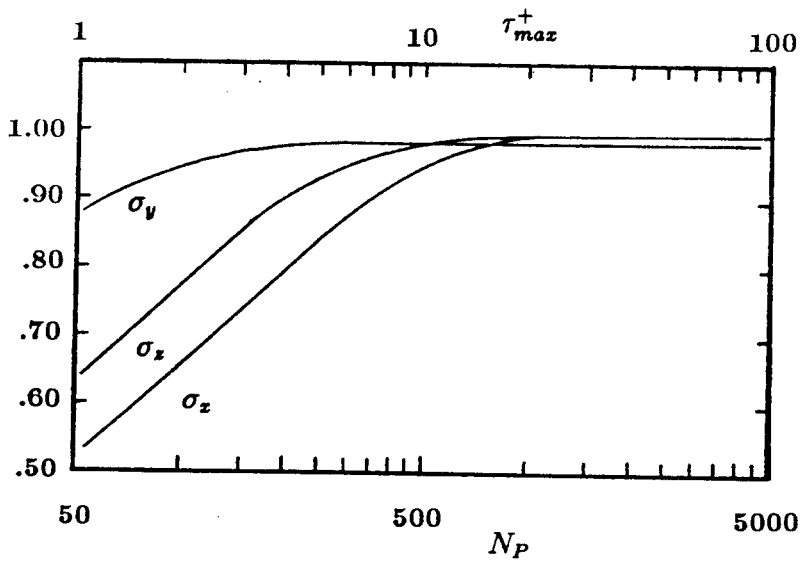


Figure 5: Simulated turbulence intensity levels.

3.3 Time-Series At Moving Nodes

Nodes which are downstream of the point at which the turbulence is generated will effectively experience a time delay in the stochastic series of the previous section. For a node which is moving, this delay changes as a function of time since the time delay is solely a function of streamwise position. In order to enter the calculated stochastic data set (V^+, τ^+) with the proper value of τ^+ the following transformation must be made:

$$\tau^+(x) = \tau^+(x_{so}) - \Delta\tau_D^+ . \quad (11)$$

Here, the value of $\tau^+(x_{so})$ is equal to $t\bar{U}/h$, where t is the actual time. The quantity $\Delta\tau_D^+$ is the non-dimensional time delay and x_{so} is the streamwise distance from the vertical axis of the turbine to the point at which the turbulence is generated (see Figure 3). The position x_{so} should be upstream of the rotor blade path. In other words, x_{so} should be less than or equal to the negative of the rotor radius r in a given horizontal plane ($x_{so} \leq -r$).

The time delay $\Delta\tau_D^+$, at any position x , is obtained from the integral:

$$\Delta\tau_D^+ = \frac{\bar{U}}{h} \int_{x_{so}}^x \frac{dx}{U} . \quad (12)$$

Here, the velocity distribution $U(x)$ is of the form which is indicated in Figure 3. Using this velocity distribution in Equation 12 yields a formulation for $\Delta\tau_D^+$ of:

$$\Delta\tau_D^+ = \frac{r}{h} \left[\frac{1}{c_2} \ln(c_1 + c_2 \frac{x}{r}) - \frac{x_{so}}{r} - 1 \right] . \quad (13)$$

This equation is valid in the region of interest for the moving nodes ($-r \leq x \leq r$). The coefficients c_1 and c_2 are a function of the wake velocity U_W and are given by:

$$\begin{aligned} c_1 &= \frac{1}{2} \left(\frac{U_W}{\bar{U}} + 1 \right) \\ c_2 &= \frac{1}{2} \left(\frac{U_W}{\bar{U}} - 1 \right) . \end{aligned} \quad (14)$$

As noted previously, the value of $\tau^+(x_{so})$ in Equation 11 is equal to $t\bar{U}/h$, where t is the time. The time t can be expressed as the product of the number of time increments N_T and the time increment Δt . It is convenient to non-dimensionalize the time t by the maximum rotor radius R and the "wind velocity" U_∞ . In other words, $t^+ \equiv tU_\infty/R$. Here, U_∞ is an arbitrary reference velocity which is used to define the "tip-to-wind speed ratio." The time increment Δt^+ can be expressed in terms of the number of time increments per revolution of the rotor N_{TI} and the tip speed of the rotor U_T by:

$$\Delta t^+ = \frac{2\pi U_\infty}{N_{TI} U_T} . \quad (15)$$

Therefore the value of $\tau^+(x_{so})$ may be calculated from:

$$\tau^+(x_{so}) = \frac{2\pi R N_T U_\infty \bar{U}}{h N_{TI} U_T U_\infty} . \quad (16)$$

In the VSTOC simulation, the positions of all specified nodes are calculated and used in Equations 13 and 11 to obtain $\tau^+(x)$ values at a particular time. Values of the turbulence velocities u', v', w' are then obtained from the data set (V^+, τ^+) by interpolation. This procedure is then repeated at each time step. In some cases τ^+ will be negative or greater than τ_{max}^+ . Since the Fourier series is periodic, these “out-of-range” values are simply shifted by multiples of τ_{max}^+ into the first period of the series. It should also be noted that the VSTOC simulation uses the same number of points to calculate the τ^+ series and the t^+ series. This implies that in order for the t^+ series to use all of the information in the τ^+ series, in a non-repetitive way, the following condition should be met:

$$\Delta\tau^+ \approx \frac{R}{h} \frac{\bar{U}}{U_\infty} \Delta t^+ \quad (17)$$

As was noted earlier, the time increment $\Delta\tau^+$ is equal to 0.02 whereas the time increment Δt^+ is given by Equation 15. Obviously, this condition cannot be met for all nodes on the rotor since \bar{U}/h is in general not a constant. However, the condition should be made to apply somewhere in the vicinity of the rotor equator.

In order to illustrate the use of the VSTOC simulation, a simple example will be given. In Figure 6 a two-node problem is illustrated. Nodes 1 and 2 are moving with the rotor while node 3 is fixed at the streamwise location where the turbulence is generated. In this particular simulation, nodes 1 and 2 are moving at a tangential velocity U_T which is 3.14 times the reference windspeed U_∞ , the wake velocity U_w is equal to \bar{U} , \bar{U} in turn is equal to U_∞ , the local radius r is equal to the maximum rotor radius R , and the turbulence intensity in the streamwise direction is 25-percent. There are 50 time steps per revolution, with a total of 1,000 steps. The simulation starts with the rotor angle θ equal to 0-deg. A “seed number” for the random number generator associated with producing a random phase angle is required. The seed number in this simulation was chosen as 0.5.

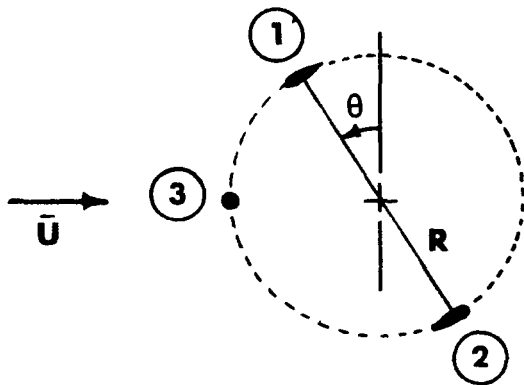


Figure 6: Node locations for example VSTOC simulation.

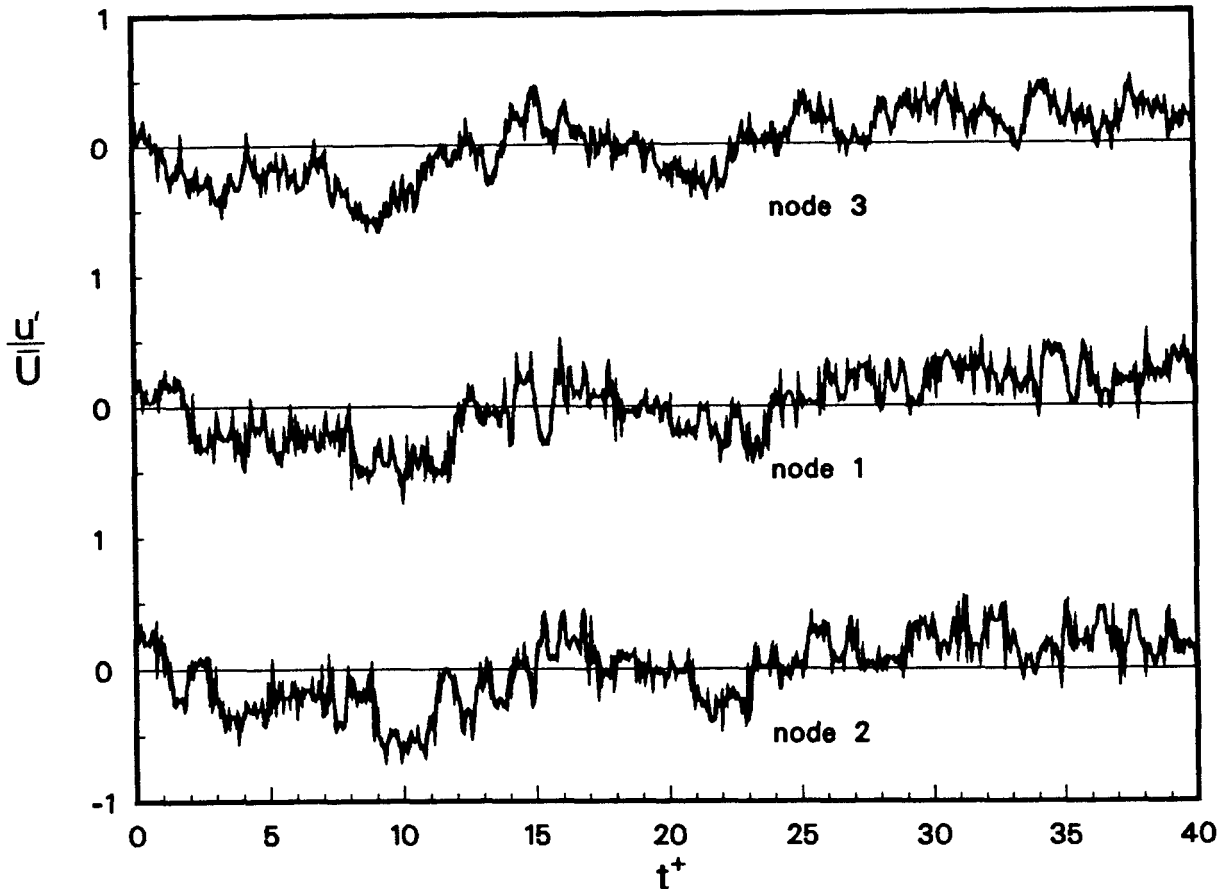


Figure 7: Streamwise wind-velocity fluctuations at rotating nodes.

In Figure 7 the streamwise turbulence component u'/\bar{U} is given for the three nodes. At first glance, the turbulence signatures are quite similar. After closer examination, however, it is clear that the signals at nodes 1 and 2 contain additional oscillations which are at the rotational frequency of the rotor (the period Δt^+ for one revolution is 2.0).

In order to gain a clearer understanding of the effect of observations from a moving node in a field of turbulence, it is useful to produce a turbulence signal generated at the fixed node 3 which has a single frequency. In Figure 8, a sinusoidal turbulence signal is introduced into the flow at node 3 and allowed to convect downstream. In this case, the frequency of the sinusoidal turbulence is lower than the rotational frequency. Two different values of U_w were chosen to show the effect of flow retardation on the turbulence observed from the moving nodes. As can be seen in Figure 8 there is a significant oscillation introduced for the moving nodes at the rotational frequency of the rotor (the rotational frequency is the same as in Figure 6). The amplitude of these secondary oscillations is a function of the slope of the turbulent input signal. This implies that secondary oscillations are amplified with increasing turbulence frequencies so long as they are less than the rotational frequency. When one observes the effect of flow retardation on the secondary oscillations, it is clear that the amplitude of

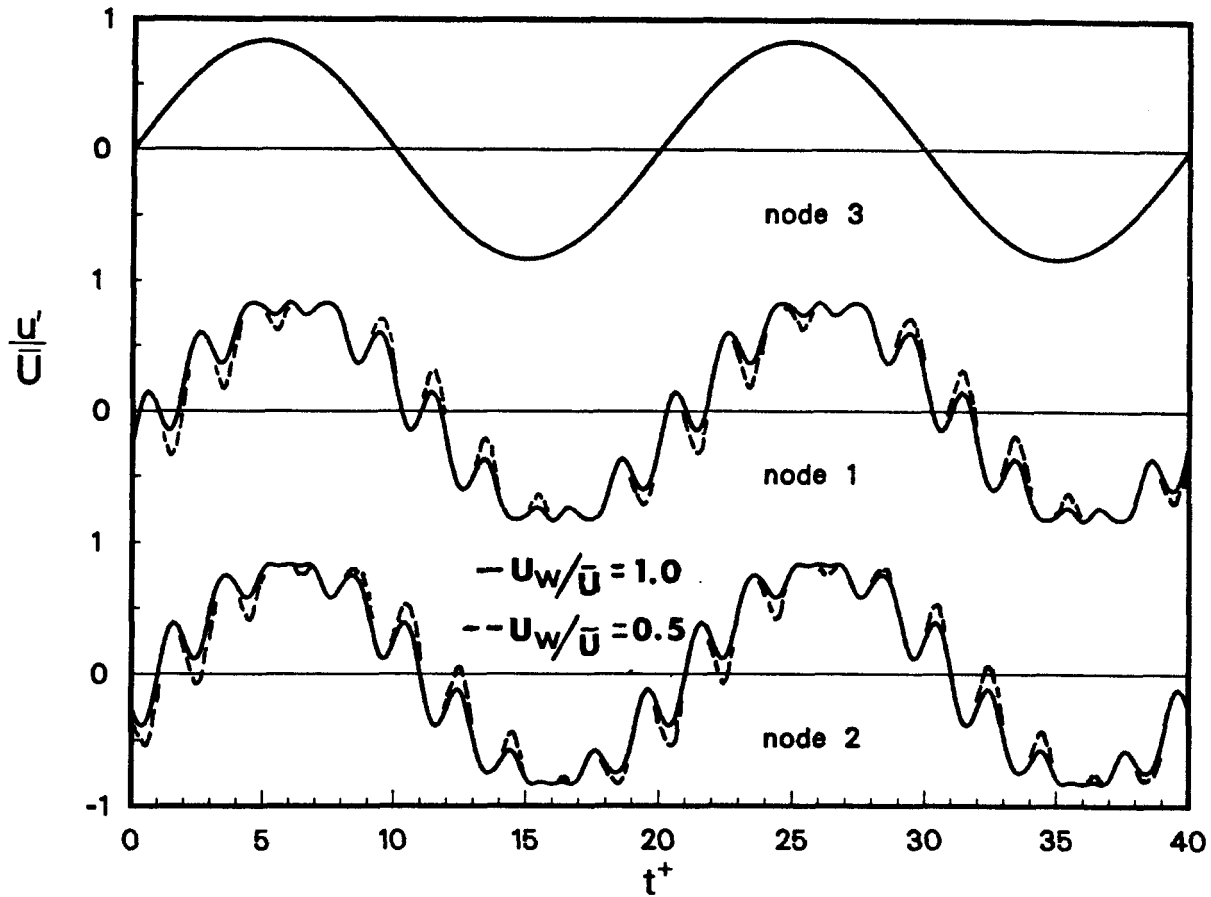


Figure 8: Moving node response to sinusoidal input velocity.

these oscillations is increased by increased flow retardation. It can, in fact, be shown from Equation 13 that the excursion in $\Delta\tau_D^+$ during each rotor revolution is increased as U_w/\bar{U} decreases, going to infinity as U_w/\bar{U} approaches zero. This explains the indicated amplification and also suggests that as $\Delta\tau_D^+$ excursions exceed the period of a particular turbulence wavelength that the energy in that frequency band is shifted to a higher frequency band. Therefore, it appears that flow retardation effects are essential in stochastic simulations for VAWTS, at least in the medium to high tip-to-wind speed range.

4 VSTOC SUBROUTINE

4.1 Subroutine Description

The VSTOC subroutine calls three other subroutines and manages their input and output. The first subroutine called, generates a non-dimensional stochastic turbulent wind series whose time base is τ^+ . This subroutine is thus designated as the TAU Series (TAUS) subroutine. TAUS in turn calls two FFT subroutines which are a part of the SLATEC library. The second subroutine called by VSTOC calculates the streamwise or X positions of the moving rotor BLADE nodes at various times and is thus called XBLADE. The third subroutine (TIMES) generates TIME Series for the same moving blade nodes. A schematic of the subroutine organization is shown in Figure 9. A more detailed description of each subroutine is given in the following paragraphs.

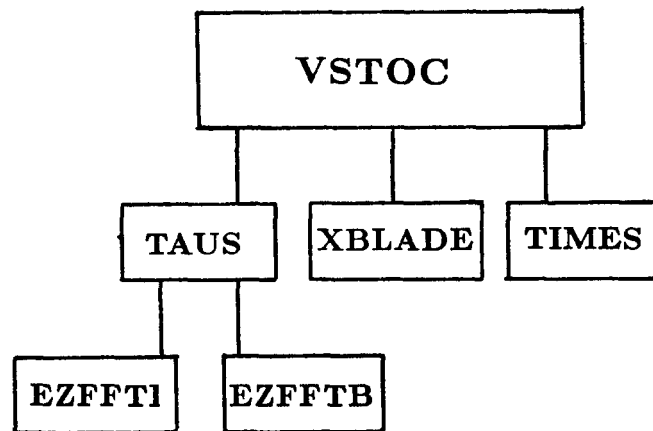


Figure 9: Subroutine organization.

In lines 6-8 of the VSTOC subroutine listed in Section 7.1, values of $CC(1)$, $CC(2)$, and $CC(3)$ are defined. These parameters are the same as C associated with Equation 3. Values of $ETA0X$, $ETA0Y$, and $ETA0Z$ given in lines 9-11 are the same as η_0 in Equation 1. $TMAX$ in line 12 is equivalent to τ_{max}^+ and is related to NP (N_P) according to Equations 9 and 10. In lines 13-15 the subroutine TAUS is called three times for the calculation of the velocity fluctuation components u'/σ , v'/σ , and w'/σ . These parameters appear as VX , VY , and VZ in the subroutine arguments. A seed number (SEED) is required as input to the TAUS subroutine in order to initiate a random number generator. In lines 18-20, three arrays are defined ($UPR(NOD+2,NT)$, etc.) which essentially represent the data set (V^+, τ^+) . In these equations, NOD is the number of specified moving nodes and $NT=N_T$ is the time increment number which is related to τ^+ . In line 21, the subroutine XBLADE is called. Input to XBLADE

includes the number of time increments per rotor revolution $NTI=N_{TI}$ and the parameter XSO. XSO is equal to the streamwise position x_{s0} at which the turbulence is generated divided by the rotor radius R . Node geometry is input in terms of the radius ratio RR, where $RR=r/R$, and the initial angular position BTHET. The output from XBLADE is an array of streamwise nodal positions (XB) at a particular time. Here, $XB = x_b/R$. Lines 23-25 yield geometry information for a fixed reference node located at a height $H=h/R$ and a streamwise position $XSO=x_{s0}/R$. The wake velocity ($UW = U_w/\bar{U}$) and the mean velocity ($UB = \bar{U}/U_\infty$) are given in lines 26 and 27 for the same reference node. USO is the value of \bar{U}/U_∞ at the reference node. In lines 28-30 the subroutine TIMES is called in order to generate the velocity fluctuation components u'/σ , v'/σ , and w'/σ at each node. These fluctuations correspond to UNP, VNP, and WNP. The tip-to-wind speed ratio $UT=U_T/U_\infty$ is also required as an input into TIMES. The value of $SIGMA=\sigma/\bar{U}$ is obtained in lines 31-36 for the three components of velocity. If SIGMA is input as a negative number, then it is calculated according to Equation 3. On the other hand, if SIGMA is input as a positive number, lines 31-36 yield a value of SIGMA equal to that number. Finally, the actual turbulent velocity fluctuations u'/\bar{U} , v'/\bar{U} , and w'/\bar{U} are calculated as UPR, VPR, and WPR in lines 38-40.

The subroutine TAUS is used to generate a stochastic wind series from the spectral model. In line 4, the value of $AZERO=A_0^+$ is set equal to zero since TAUS generates fluctuations about the mean velocity \bar{U} . Line 5 represents Equation 9 where $DELETA=\Delta\eta^+$. The subroutine EZFFTI, which is called in line 6, is required to initialize the subroutine EZFFTB. These two subroutines, which are a part of the SLATEC math library, form a Fast Fourier Transform package used to convert the spectral data into a time-series. The array WSAVE, which is placed in the argument of EZFFTI, is a work array which must have dimensions of at least $3NP+15$. In the present case, the maximum value of NP is 5,000. Line 8 calculates $ETA=\eta_j^+$ based on $\Delta\eta^+$. The random phase angle $PHI=\phi_j$ is calculated in line 9. A random number generator (RAND), which is available from the SLATEC library, is used in the calculation of PHI. The argument for RAND, which is denoted by SEED, must initially be set equal to some value between 0.0 and 1.0. In line 11, the spectral power density $F=F_j$ is calculated based on Equation 4. The coefficients $A=A_j^+$ and $B=B_j^+$ are calculated in lines 12 and 13 according to Equation 8. Finally, the FFT package is used in line 15 to calculate $VSIG=V^+/\sigma^+$ according to Equation 6.

The subroutine XBLADE is used to calculate the streamwise positions of each moving node at a given time. In line 4, the angular position of the rotor is calculated based on the time increment number NT and the number of time increments per revolution of the rotor NTI. In line 6, the initial angular position of node I, in degrees, is given by BTHET(I) whereas BTHETR is the angular position in radians. In line 7, the streamwise position $XB=x_b/R$ is obtained for all nodes. As indicated in line 5, the number of nodes is equal to NOD.

The subroutine TIMES is used to obtain the velocity fluctuation components u'/σ , v'/σ , and w'/σ at each node. The parameter VPR corresponds to either u'/σ , v'/σ , or w'/σ , depending upon the parameters placed in the TIMES subroutine argument list

from VSTOC. TMAX in line 4 is equivalent to τ_{max}^+ and is related to NP (N_P) according to Equations 9 and 10. The parameter RRX is equal to r/R . In line 5, C1 represents c_1 and UWX= U_w/\bar{U} from Equation 14. In line 7, C2 is equal to c_2R/r . Line 7 is equivalent to the second part of Equation 14. In lines 8-21 the parameter DELTAU= $\Delta\tau_D^+$ is calculated using Equation 12. In these lines, XX is the streamwise position x/R and HX is the elevation h/R . Line 22 represents a combination of Equations 11 and 16. TAU is equal to $\tau^+(x)$ while UBX= \bar{U}/U_∞ . Lines 23-26 shift “out of range” values of τ^+ into the first period of the Fourier series. Lines 27-32 provide interpolation logic to obtain the proper value of VPR=(u'/σ , v'/σ , or w'/σ) from one of the arrays represented by VS. The arrays VS=(VX, VY, or VZ) were generated previously by the subroutine TAUS.

4.2 Input-Output

The input-output will be discussed with regard to the VSTOC subroutine listed in section 7.1 and the VSTOC with input-output drivers listed in section 7.2. In general, the user will only be interested in the input-output characteristics of the basic VSTOC subroutine. For completeness, however, a brief description of VSTOC with input-output drivers will be given.

In the basic VSTOC subroutine, there are 15 parameters in the argument list. The input consists of 9 single-valued parameters and 6 single subscripted arrays. The output consists of 3 double subscripted arrays. The input argument list can be described as follows:

- NOD $\equiv N_{NODES}$ - an integer which value specifies the number of moving nodes on the rotor. Its maximum value is 98.
- NTI $\equiv N_{TI}$ - an integer which specifies the number of time increments per revolution of the rotor.
- NP $\equiv N_P$ - an integer which specifies the number of time increments in the time-series. Its value should be between 1,000 and 5,000.
- UT $\equiv U_T/U_\infty$ - a real variable which is the tip-to-wind speed ratio.
- HO $\equiv h_o/R$ - a real variable which is the ratio of the roughness height to the rotor radius.
- XSO $\equiv x_{so}/R$ - a real variable which is the ratio of the streamwise position at which the turbulence is generated to the rotor radius. This variable also specifies the streamwise position of the fixed node.
- HSO $\equiv h_{so}/R$ - a real variable which is the ratio of the height above ground at the fixed node to the rotor radius.

- $USO \equiv \bar{U}_{so}/U_{\infty}$ - a real variable which is the ratio of the upstream wind velocity at the fixed node to the reference wind velocity.
- $SIGMA(K) \equiv \sigma_k$ - a real array with three components ($k = 1, 2, 3$) which specifies the x , y , and z components of the turbulence intensity. The values are specified as positive decimal fractions unless the user wants the subroutine to calculate values internally. In that case, any set of negative real values may be input.
- $SEED \equiv Seed$ - a real variable which is arbitrarily chosen between 0.0 and 1.0. Each choice will produce a different stochastic series from the same spectral data.
- $BTHET(I) \equiv \theta_{B_i}$ - a real array which specifies the initial angular position of node i when $t^+ = 0.0$. The maximum value of I is 98.
- $RR(I) \equiv r_i/R$ - a real array which is the radius of node i with respect to the vertical axis divided by the rotor radius (maximum).
- $H(I) \equiv h_i/R$ - a real array which specifies the height above ground of node i divided by the rotor radius.
- $UB(I) \equiv \bar{U}_i/U_{\infty}$ - a real array which specifies the average wind velocity upstream of node i divided by the reference wind velocity.
- $UW(I) \equiv U_{W_i}/\bar{U}_i$ - a real array which specifies the wake velocity downstream of node i divided by the average wind velocity upstream of node i .

The output consists of non-dimensional three-component velocity fluctuations for each of the nodes, including the fixed node. These double subscripted real arrays represent the calculated values of the streamwise velocity fluctuations as a function of time. They are non-dimensionalized by the average upstream velocity at the appropriate node i . The subscript j denotes the time step number. The non-dimensional time t^+ is obtained from the product of j and Δt^+ which is given in Equation 15. The fixed node is assigned a node number $I=NOD+1$. The output argument list is given by:

- $UPR(I,J) \equiv u'_{i,j}/\bar{U}_i$ - a real array which represents the non-dimensional streamwise velocity fluctuation at each node as a function of time.
- $VPR(I,J) \equiv v'_{i,j}/\bar{U}_i$ - a real array which represents the non-dimensional vertical velocity fluctuation at each node as a function of time.
- $WPR(I,J) \equiv w'_{i,j}/\bar{U}_i$ - a real array which represents the non-dimensional lateral velocity fluctuation at each node as a function of time.

The VSTOC program with input-output drivers, as listed in section 7.2, was written specifically to demonstrate the features of the VSTOC subroutine. An input file whose name is VSTOC.INPUT is required for execution of the program. Tabular output, which includes input parameters as well as calculated results, is written to a file

whose name is VSTOC.OUTPUT. The calculated results, which are tabulated, consist of the of the first 40 values of u'/σ , v'/σ , and w'/σ in the τ^+ series and the first 40 values of u'/\bar{U} , v'/\bar{U} , and w'/\bar{U} in the t^+ series at each node. In the τ^+ series, the parameters SIGMAX, SIGMAY, and SIGMAZ are simulated *rms* values of u'/σ , v'/σ , and w'/σ respectively. In the t^+ series, the parameters SIGMAU, SIGMAV, and SIGMAW are simulated *rms* values of u'/\bar{U} , v'/\bar{U} , and w'/\bar{U} respectively. Graphical results are contained in a file named FOR077.DAT. Typical output from this program is included at the end of the program listing in section 7.2. The format of the input file VSTOC.INPUT is as shown in Table 1.

Table 1: Input to VSTOC with input-output drivers

Record	Parameter	Format
1	NOD	I10
2	NTI	I10
3	NP	I10
4	UT	F10.4
5	HO	F10.4
6	XSO	F10.4
7	HSO	F10.4
8	USO	F10.4
9	SIGMA(1)	F10.4
10	SIGMA(2)	F10.4
11	SIGMA(3)	F10.4
12	SEED	F10.4
13	BTHET(1),RR(1),H(1),UB(1),UW(1)	5F10.4
14	BTHET(2),RR(2),H(2),UB(2),UW(2)	5F10.4
.	.	.
.	.	.
.	.	.
12+NOD	BTHET(NOD),RR(NOD),H(NOD),UB(NOD),UW(NOD)	5F10.4

5 SUMMARY AND CONCLUSIONS

A stochastic wind simulation for VAWTs (VSTOC) has been developed which yields turbulent wind-velocity fluctuations for rotationally sampled points. This allows three-component wind-velocity fluctuations to be simulated at specified nodal points on the wind-turbine rotor. A first-order convection scheme is used which accounts for the decrease in streamwise velocity as the flow passes through the wind-turbine rotor. The VSTOC simulation is independent of the particular analytical technique used to predict the aerodynamic characteristics of the turbine since only time-averaged centerline wake velocities are required as input into VSTOC from a given VAWT aerodynamic code. This information is obtainable from virtually all known VAWT aerodynamic codes. The most efficient utilization of the VSTOC subroutine is to use it in a post processor to a VAWT aerodynamic code. The VAWT aerodynamic code is required to calculate only the deterministic periodic flow field, independent of wind turbulence. Deterministic flow velocities from the VAWT aerodynamic module are mixed with the stochastic flow velocities from VSTOC and used in a VAWT performance module to predict blade loading.

There are two major conclusions that should be emphasized as a result of this work. They are as follows:

- The inclusion of flow retardation through the rotor is essential, since flow retardation significantly affects the transfer of turbulent energy from lower frequencies into higher frequencies at the moving rotor blade nodes.
- The concept of using three computational modules (VAWT aero., VSTOC, and VAWT perf.) for predicting blade loading in turbulent winds should yield good results at all tip-to-wind speed ratios since flow perturbations due to the rotor are small when the aerodynamics are non-linear (ie. aerodynamic stall at low tip-to-wind speed ratios). This method is very efficient with respect to minimizing computer time.

6 REFERENCES

- [1] Strickland, J. H., "A Review of Aerodynamic Analysis Methods for Vertical Axis Wind Turbines," Proceedings of the 5th ASME Wind Energy Symposium, 1986, pp.7-17.
- [2] Sheldahl, R. E., "Comparison of Field and Wind Tunnel Darrieus Turbine Data," Sandia National Laboratories Report SAND80-2469, January 1981.
- [3] Veers, P. S., "Modeling Stochastic Wind Loads on Vertical Axis Wind Turbines," Sandia National Laboratories Report SAND83-1909, September 1984.
- [4] Strickland, J. H., "The Darrieus Turbine: A Performance Prediction Model Using Multiple Streamtubes," Sandia National Laboratories Report SAND75-0431, October 1975.
- [5] George, R. L., "Simulation of Winds As Seen By a Rotating Vertical Axis Wind Turbine Blade," Pacific Northwest Laboratory Report PNL-4914, February 1984.
- [6] Powell, D. C., and Connell, J. R., "A Model For Simulating Rotational Data For Wind Turbine Applications," Pacific Northwest Laboratory Report PNL-5857, April 1986.
- [7] Strickland, J. H. and Goldman, A. L., "Preliminary Work Concerning the Near-Wake Structure of the Darrieus Turbine," *AIAA Journal of Energy*, Vol.5, No.2, 1981, pp.94-98.
- [8] Templin, R. J., "Aerodynamic Performance Theory for the NRC Vertical-Axis Wind Turbine," National Research Council of Canada Report LTR-LA-160, June 1974.
- [9] Strickland, J. H., Webster, B. T., and Nguyen, T., "A Vortex Model of the Darrieus Turbine: An Analytical and Experimental Study," *Journal of Fluids Engineering*, Vol.101, December 1979, pp.500-505.
- [10] Frost, W., Long, B. H., and Turner, R. E., "Engineering Handbook on the Atmospheric Environmental Guidelines for use in Wind Turbine generator Development," NASA Technical Paper 1359, 1978.

7 PROGRAM LISTING

7.1 VSTOC Subroutine

```
01     SUBROUTINE VSTOC(SEED,NTI,NP,UT,UB,UW,H,HO,XSO,HSO,USO,SIGMA,
02     $NOD,BTHET,RR,UPR,VPR,WPR)
03     DIMENSION SIGMA(3),CC(3),XB(100),UPR(100,5000),VPR(100,5000),
04     $WPR(100,5000),VX(5000),VY(5000),VZ(5000),RR(100),BTHET(100),
05     $H(100),UB(100),UW(100)
06     CC(1)=1.00
07     CC(2)=0.52
08     CC(3)=0.64
09     ETAOX=.0144
10     ETAOY=.0962
11     ETAOZ=.0265
12     TMAX=FLOAT(NP)/50.0
13     CALL TAUS(NP,TMAX,VX,ETAOX,SEED)
14     CALL TAUS(NP,TMAX,VY,ETAOY,SEED)
15     CALL TAUS(NP,TMAX,VZ,ETAOZ,SEED)
16 40  CONTINUE
17     DO 20 NT=1,NP
18     UPR(NOD+2,NT)=VX(NT)
19     VPR(NOD+2,NT)=VY(NT)
20     WPR(NOD+2,NT)=VZ(NT)
21     CALL XBLADE(NOD,NTI,NT,XB,XSO,RR,BTHET)
22     DO 30 I=1,NOD+1
23     XB(NOD+1)=XSO
24     H(NOD+1)=HSO
25     RR(NOD+1)=-XSO
26     UW(NOD+1)=1.0
27     UB(NOD+1)=USO
28     CALL TIMES(VX,NT,NTI,NP,UT,UB(I),UW(I),H(I),XB(I),XSO,RR(I),UNP)
29     CALL TIMES(VY,NT,NTI,NP,UT,UB(I),UW(I),H(I),XB(I),XSO,RR(I),VNP)
30     CALL TIMES(VZ,NT,NTI,NP,UT,UB(I),UW(I),H(I),XB(I),XSO,RR(I),WNP)
31     DO 10 J=1,3
32     IF(SIGMA(J).LT.0.0) THEN
33     SIGMA(J)=CC(J)/LOG(H(I)/HO+1.0)
34     ELSE
35     SIGMA(J)=SIGMA(J)
36     END IF
37 10  CONTINUE
```

```

38     UPR(I,NT)=SIGMA(1)*UNP
39     VPR(I,NT)=SIGMA(2)*VNP
40     WPR(I,NT)=SIGMA(3)*WNP
41  30  CONTINUE
42  20  CONTINUE
43     RETURN
44     END

```

```

01     SUBROUTINE TAUS(NP,TMAX,VSIG,ETAO,SEED)
02     DIMENSION VSIG(5000),A(2500),B(2500),WSAVE(15015)
03     PI=4.0*ATAN(1.0)
04     AZERO=0.0
05     DELETA=1.0/TMAX
06     CALL EZFFTI(NP,WSAVE)
07     DO 20 I=1,NP/2
08     ETA=DELETA*(FLOAT(I)-0.5)
09     PHI=2.0*PI*RAND(SEED)
10     SEED=0.0
11     F=0.171/(ETAO*(1.0+0.164*(ETA/ETAO)**(5.0/3.0)))
12     A(I)=SQRT(2.0*F*DELETA)*SIN(PHI)
13     B(I)=SQRT(2.0*F*DELETA)*COS(PHI)
14  20  CONTINUE
15     CALL EZFFTB(NP,VSIG,AZERO,A,B,WSAVE)
16     RETURN
17     END

```

```

01     SUBROUTINE XBLADE(NOD,NTI,NT,XB,XSO,RR,BTHET)
02     DIMENSION RR(100),BTHET(100),XB(100)
03     PI=4.0*ATAN(1.0)
04     RTHET=FLOAT(NT)*2.0*PI/FLOAT(NTI)
05     DO 10 I=1,NOD
06     BTHETR=BTHET(I)*PI/180.0
07     XB(I)=-RR(I)*SIN(RTHET+BTHETR)
08  10  CONTINUE
09     RETURN
10     END

```

```

01     SUBROUTINE TIMES(VS,NT,NTI,NP,UT,UBX,UWX,HX,XX,XSO,RRX,VPR)
02     DIMENSION VS(5000)
03     PI=4.0*ATAN(1.0)
04     TMAX=FLOAT(NP)/50.0
05     C1=(1.0+UWX)/2.0
06     IF(RRX.EQ.0.0) RRX=.001
07     C2=-(1.0-UWX)/(2.0*RRX)
08     IF(C2.EQ.0.0) THEN
09     DELTAU=(XX-XSO)/HX
10     GO TO 30
11     ELSE
12     END IF
13     IF(XX.LE.-RRX) THEN
14     DELTAU=(XX-XSO)/HX
15     ELSE
16     IF(XX.LE.RRX) THEN
17     DELTAU=(-RRX-XSO+LOG(C1+C2*XX)/C2)/HX
18     ELSE
19     DELTAU=(-RRX-XSO+LOG(C1+C2*RRX)/C2+(XX-RRX)/UWX)/HX
20     END IF
21     END IF
22 30  TAU=2.0*PI*UBX*FLOAT(NT)/(UT*FLOAT(NTI)*HX)-DELTAU
23 10  IF(TAU.LT.0.0)TAU=TAU+TMAX
24     IF(TAU.LT.0.0) GO TO 10
25 20  IF(TAU.GE.TMAX)TAU=TAU-TMAX
26     IF(TAU.GE.TMAX) GO TO 20
27     N=INT(50.0*TAU)
28     IF(N.EQ.0) THEN
29     VPR=VS(NP)+(50.0*TAU)*(VS(1)-VS(NP))
30     ELSE
31     VPR=VS(N)+(50.0*TAU-FLOAT(N))*(VS(N+1)-VS(N))
32     END IF
33     RETURN
34     END

```

7.2 VSTOC With Input-Output Drivers

```
DIMENSION SIGMA(3),BTHET(100),RR(100),H(100),UB(100),UW(100),
$UPR(100,5000),VPR(100,5000),WPR(100,5000)
CALL VSTART(1.013,5)
CALL INPUT(SEED,NTI,NP,UT,UB,UW,H,HO,XSO,HSO,USO,SIGMA,NOD,
$BTHET,RR)
CALL VSTOC(SEED,NTI,NP,UT,UB,UW,H,HO,XSO,HSO,USO,SIGMA,NOD,
$BTHET,RR,UPR,VPR,WPR)
NPP=40
CALL OUTPUT(NOD,NTI,NP,NPP,UT,UPR,VPR,WPR,BTHET)
CALL DONEPL
STOP
END
```

```
SUBROUTINE INPUT(SEED,NTI,NP,UT,UB,UW,H,HO,XSO,HSO,USO,SIGMA,
$NOD,BTHET,RR)
DIMENSION SIGMA(3),BTHET(100),RR(100),H(100),UB(100),UW(100)
PI=4.0*ATAN(1.0)
OPEN(UNIT=11,STATUS='OLD',FILE='VSTOC.INPUT')
OPEN(UNIT=12,STATUS='NEW',FILE='VSTOC.OUTPUT')
READ(11,3)NOD,NTI,NP,UT,HO,XSO,HSO,USO,SIGMA(1),SIGMA(2),
$SIGMA(3),SEED
WRITE(12,15)SEED,NTI,NP,UT,HO,XSO,HSO,USO<SIGMA(1),SIGMA(2),
$SIGMA(3)
DO 2 I=1,NOD
READ(11,13)BTHET(I),RR(I),H(I),UB(I),UW(I)
WRITE(12,17)I,BTHET(I),RR(I),H(I),UB(I),UW(I)
2 CONTINUE
WRITE(12,19)
3 FORMAT(I10,/,I10,/,I10,/,F10.4,/,F10.4,/,F10.4,/,F10.4,/,
$F10.4,/,F10.4,/,F10.4,/,F10.4,/,F10.4 )
13 FORMAT(5F10.4)
```

```

15  FORMAT('1',
$      /25X,'*****',
$      /25X,'*          GENERAL INPUT          *',
$      /25X,'*****',
$      /25X,'* SEED =',F9.3,' *',
$      /25X,'* NTI =',I5,' *',
$      /25X,'* NP =',I5,' *',
$      /25X,'* UT =',F9.3,' *',
$      /25X,'* HO =',F9.3,' *',
$      /25X,'* XSO =',F9.3,' *',
$      /25X,'* HSO =',F9.3,' *',
$      /25X,'* USO =',F9.3,' *',
$      /25X,'* SIGX =',F9.3,' *',
$      /25X,'* SIGY =',F9.3,' *',
$      /25X,'* SIGZ =',F9.3,' *',
$      /25X,'*****',////
$/10X,'*****',
$/10X,'*
$          NODAL INPUT *',
$/10X,'*****',
$/10X,'* NODE   THETA       R           H           UB           UW *')
17  FORMAT(10X,'* ',I3,3X,F8.4,2X,F8.4,2X,F8.4,2X,F8.4,2X,F8.4' *')
19  FORMAT(
$ 10X,'*****')
RETURN
END

```

```

SUBROUTINE VSTOC(SEED,NTI,NP,UT,UB,UW,H,HO,XSO,HSO,USO,SIGMA,
$NOD,BTHET,RR,UPR,VPR,WPR)
  DIMENSION SIGMA(3),CC(3),XB(100),UPR(100,5000),VPR(100,5000),
$WPR(100,5000),VX(5000),VY(5000),VZ(5000),RR(100),BTHET(100),
$H(100),UB(100),UW(100)
  CC(1)=1.00
  CC(2)=0.52
  CC(3)=0.64
  ETAOX=.0144
  ETAOY=.0962
  ETAOZ=.0265
  TMAX=FLOAT(NP)/50.0
  CALL TAUS(NP,TMAX,VX,ETAOX,SEED)
  CALL TAUS(NP,TMAX,VY,ETAOY,SEED)
  CALL TAUS(NP,TMAX,VZ,ETAOZ,SEED)
40  CONTINUE
  DO 20 NT=1,NP
    UPR(NOD+2,NT)=VX(NT)
    VPR(NOD+2,NT)=VY(NT)
    WPR(NOD+2,NT)=VZ(NT)
    CALL XBLADE(NOD,NTI,NT,XB,XSO,RR,BTHET)
    DO 30 I=1,NOD+1
      XB(NOD+1)=XSO
      H(NOD+1)=HSO
      RR(NOD+1)=-XSO
      UW(NOD+1)=1.0
      UB(NOD+1)=USO
      CALL TIMES(VX,NT,NTI,NP,UT,UB(I),UW(I),H(I),XB(I),XSO,RR(I),UNP)
      CALL TIMES(VY,NT,NTI,NP,UT,UB(I),UW(I),H(I),XB(I),XSO,RR(I),VNP)
      CALL TIMES(VZ,NT,NTI,NP,UT,UB(I),UW(I),H(I),XB(I),XSO,RR(I),WNP)
    DO 10 J=1,3
      IF(SIGMA(J).LT.0.0) THEN
        SIGMA(J)=CC(J)/LOG(H(I)/HO+1.0)
      ELSE
        SIGMA(J)=SIGMA(J)
      END IF
10  CONTINUE

```

```

UPR(I,NT)=SIGMA(1)*UNP
VPR(I,NT)=SIGMA(2)*VNP
WPR(I,NT)=SIGMA(3)*WNP
30 CONTINUE
20 CONTINUE
RETURN
END

```

```

SUBROUTINE TAUS(NP,TMAX,VSIG,ETAO,SEED)
DIMENSION VSIG(5000),A(2500),B(2500),WSAVE(15015)
PI=4.0*ATAN(1.0)
AZERO=0.0
DELETA=1.0/TMAX
CALL EZFFTI(NP,WSAVE)
DO 20 I=1,NP/2
ETA=DELETA*(FLOAT(I)-0.5)
PHI=2.0*PI*RAND(SEED)
SEED=0.0
F=0.171/(ETAO*(1.0+0.164*(ETA/ETAO)**(5.0/3.0)))
A(I)=SQRT(2.0*F*DELETA)*SIN(PHI)
B(I)=SQRT(2.0*F*DELETA)*COS(PHI)
20 CONTINUE
CALL EZFFTB(NP,VSIG,AZERO,A,B,WSAVE)
RETURN
END

```

```

SUBROUTINE XBLADE(NOD,NTI,NT,XB,XSO,RR,BTHET)
DIMENSION RR(100),BTHET(100),XB(100)
PI=4.0*ATAN(1.0)
RTHET=FLOAT(NT)*2.0*PI/FLOAT(NTI)
DO 10 I=1,NOD
BTHETR=BTHET(I)*PI/180.0
XB(I)=-RR(I)*SIN(RTHET+BTHETR)
10 CONTINUE
RETURN
END

```

```

SUBROUTINE TIMES(VS,NT,NTI,NP,UT,UBX,UWX,HX,XX,XSO,RRX,VPR)
DIMENSION VS(5000)
PI=4.0*ATAN(1.0)
TMAX=FLOAT(NP)/50.0
C1=(1.0+UWX)/2.0
IF(RRX.EQ.0.0) RRX=.001
C2=-(1.0-UWX)/(2.0*RRX)
IF(C2.EQ.0.0) THEN
DELTAU=(XX-XSO)/HX
GO TO 30
ELSE
END IF
IF(XX.LE.-RRX) THEN
DELTAU=(XX-XSO)/HX
ELSE
IF(XX.LE.RRX) THEN
DELTAU=(-RRX-XSO+LOG(C1+C2*XX)/C2)/HX
ELSE
DELTAU=(-RRX-XSO+LOG(C1+C2*RRX)/C2+(XX-RRX)/UWX)/HX
END IF
END IF
30 TAU=2.0*PI*UBX*FLOAT(NT)/(UT*FLOAT(NTI)*HX)-DELTAU
10 IF(TAU.LT.0.0)TAU=TAU+TMAX
IF(TAU.LT.0.0) GO TO 10
20 IF(TAU.GE.TMAX)TAU=TAU-TMAX
IF(TAU.GE.TMAX) GO TO 20
N=INT(50.0*TAU)
IF(N.EQ.0) THEN
VPR=VS(NP)+(50.0*TAU)*(VS(1)-VS(NP))
ELSE
VPR=VS(N)+(50.0*TAU-FLOAT(N))*(VS(N+1)-VS(N))
END IF
RETURN
END

```

```

SUBROUTINE OUTPUT(NOD,NTI,NP,NPP,UT,UPR,VPR,WPR,BTHET)
  DIMENSION UPR(100,5000),VPR(100,5000),WPR(100,5000),BTHET(100),
$TAU(5000),TIME(5000),VX(5000),VY(5000),VZ(5000),U1(5000),
$U2(5000),U3(5000)
  PI=4.0*ATAN(1.0)
  IF(NP.LT.1000.0)THEN
    WRITE(12,11)
11  FORMAT('1',
$ //15X,'*****',
$ /15X,'*                WARNING!!!          *',
$ /15X,'*****',
$ /15X,'* RESULTS MAY BE INACCURATE FOR NP LESS *',
$ /15X,'* THAN 1000.CHECK SIMULATED SIGMAS FROM *',
$ /15X,'* NORMALIZED TAU-SERIES. THESE SHOULD *',
$ /15X,'* BE APPROXIMATELY EQUAL TO 1.00.      *',
$ /15X,'*****')
    END IF
    DELT=0.02
    SX=0.0
    SY=0.0
    SZ=0.0
    DO 50 I=1,NP
      TAU(I)=DELT*I
      TIME(I)=2.0*PI*FLOAT(I)/(FLOAT(NTI)*UT)
      VX(I)=UPR(NOD+2,I)
      VY(I)=VPR(NOD+2,I)
      VZ(I)=WPR(NOD+2,I)
      U1(I)=UPR(1,I)
      U2(I)=UPR(2,I)
      U3(I)=UPR(NOD+1,I)
      SX=SX+VX(I)*VX(I)
      SY=SY+VY(I)*VY(I)
      SZ=SZ+VZ(I)*VZ(I)
50  CONTINUE

```

```

RMSVX=SQRT(SX/FLOAT(NP))
RMSVY=SQRT(SY/FLOAT(NP))
RMSVZ=SQRT(SZ/FLOAT(NP))
WRITE(12,13)RMSVX,RMSVY,RMSVZ
13  FORMAT('1',
$    //15X,'*****',
$    /15X,'*          NORMALIZED TAU-SERIES          *',
$    /15X,'*****',
$    /15X,'*  SIGMAX=',F7.4,' *  NORMALIZED VALUES *',
$    /15X,'*  SIGMAY=',F7.4,' *          OF          *',
$    /15X,'*  SIGMAZ=',F7.4,' *          SIGMA.          *',
$    /15X,'*****',
$    /15X,'*                                          *',
$    /15X,'*          - TAU-SERIES -          *',
$    /15X,'*                                          *')
WRITE(12,17)
17  FORMAT(15X,'*  TAU',7X,'VX',8X,'VY',8X,'VZ  *')
DO 40 I=1,NPP
WRITE(12,15)TAU(I),VX(I),VY(I),VZ(I)
15  FORMAT(15X,'*  ',F6.2,2X,3F10.5,' *')
40  CONTINUE
WRITE(12,19)
19  FORMAT(15X,'*****')
CALL TAUPLOT(1000,VX,VY,VZ,TAU)
DO 30 J=1,NOD+1
SU=0.0
SV=0.0
SW=0.0
DO 10 I=1,NP
SU=SU+UPR(J,I)*UPR(J,I)
SV=SV+VPR(J,I)*VPR(J,I)
SW=SW+WPR(J,I)*WPR(J,I)
10  CONTINUE

```

```

RMSU=SQRT(SU/NP)
RMSV=SQRT(SV/NP)
RMSW=SQRT(SW/NP)
WRITE(12,3)J,RMSU,RMSV,RMSW
3  FORMAT('1',
$//15X,'*****',
$/15X,'*  NODE ',I3,'          TIME-SERIES          *',
$/15X,'*****',
$/15X,'*  SIGMAU=',F7.4,'      *  SIMULATED VALUES  *',
$/15X,'*  SIGMAV=',F7.4,'      *          OF          *',
$/15X,'*  SIGMAW=',F7.4,'      *          SIGMA.        *',
$/15X,'*****',
$/15X,'*
$/15X,'*          - TIME-SERIES -          *',
$/15X,'*
WRITE(12,7)
7  FORMAT(15X,'*  TIME',4X,'THETA',7X,'U ',8X,'V ',8X,'W      *')
DO 20 I=1,NPP
XRTHET=FLOAT(I)*360.0/FLOAT(NTI)
THET=BTHET(J)+XRTHET
THETA=AMOD(THET,360.0)
WRITE(12,5)TIME(I),THETA,UPR(J,I),VPR(J,I),WPR(J,I)
5  FORMAT(15X,'* ',F6.2,3X,F6.2,1X,3F10.5,' *')
20  CONTINUE
WRITE(12,9)
9  FORMAT(15X,'*****')
30  CONTINUE
CALL TIMPLOT(1000,U1,U2,U3,TIME)
RETURN
END

```

```

SUBROUTINE TAUPLOT(ND,VX,VY,VZ,TAU)
DIMENSION VX(5000),VY(5000),VZ(5000),TAU(5000),
$XO(2),YO(2),Y1(2),Y2(2),FYX(5000),FYY(5000),FYZ(5000)
XO(1)=0.0
XO(2)=FLOAT(ND)/50.0
YO(1)=0.0
YO(2)=0.0
Y1(1)=8.0/3.0
Y1(2)=Y1(1)
Y2(1)=-Y1(1)
Y2(2)=-Y1(1)
DO 20 I=1,ND
FYX(I)=Y1(1)+VX(I)/3.0
FYY(I)=YO(1)+VY(I)/3.0
FYZ(I)=Y2(1)+VZ(I)/3.0
20 CONTINUE
CALL RESET('ALL')
CALL MX1ALF('STANDARD','%')
CALL MX2ALF('L/CSTD','#')
CALL MX3ALF('INSTR','&')
CALL MX4ALF('MATH','@')
CALL MX5ALF('SPEC','*')
CALL MX6ALF('L/CGREEK','!')
CALL SWISSL
CALL SHDCHR(90.,1,.003,1)
CALL PAGE(11.0,8.5)
CALL NOBRDR
CALL HWROT('COMIC')
CALL HWSCAL('SCREEN')
CALL XREVTK
CALL YREVTK
CALL AREA2D(8.0,6.0)

```

```

CALL HEIGHT(.2)
CALL YAXANG(0.0)
CALL XNAME('!T&E.7H.5%+&EXHX%',17)
CALL YNAME(' ',1)
X=-0.3
Y=5.00-.07
DY=1.00
CALL MESSAG('&H.7%0&HX%',10,X,Y)
CALL MESSAG('&P1#U&U1*,&B2L1.1!S&LX',22,-0.75,5.05)
Y=Y-DY
CALL MESSAG('&H.7%4&HX%',10,X,Y)
CALL MESSAG('&P1#V&U1*,&B2L1.1!S&LX',22,-0.75,3.05)
Y=Y-2.0*DY
CALL MESSAG('&H.7%4&HX%',10,X,Y)
CALL MESSAG('&P1#W&U1*,&B2L1.1!S&LX',22,-0.75,1.05)
Y=Y-DY
CALL MESSAG('&H.7%0&HX%',10,X,Y)
CALL YINTAX
CALL XINTAX
CALL XTICKS(5)
CALL YTICKS(6)
CALL GRAF(0.0,5.0,XO(2),-4.0,4.0,4.0)
CALL FRAME
CALL CURVE(XO,YO,2,0)
CALL CURVE(XO,Y1,2,0)
CALL CURVE(XO,Y2,2,0)
CALL THKCRV(.02)
CALL CURVE(TAU,FYX,ND,0)
CALL CURVE(TAU,FYY,ND,0)
CALL CURVE(TAU,FYZ,ND,0)
CALL ENDPL(0)
RETURN
END

```

```

SUBROUTINE TIMPLOT(NDT,U1,U2,U3,TIME)
DIMENSION U1(5000),U2(5000),U3(5000),TIME(5000),
$XO(2),YO(2),Y1(2),Y2(2),FYX(5000),FYY(5000),FYZ(5000)
XO(1)=0.0
XO(2)=40.0
YO(1)=0.0
YO(2)=0.0
Y1(1)=2.0/3.0
Y1(2)=Y1(1)
Y2(1)=-Y1(1)
Y2(2)=-Y1(1)
DO 20 I=1,NDT
FYX(I)=Y1(1)+U3(I)/3.0
FYY(I)=YO(1)+U1(I)/3.0
FYZ(I)=Y2(1)+U2(I)/3.0
20 CONTINUE
CALL RESET('ALL')
CALL MX1ALF('STANDARD','%')
CALL MX2ALF('L/CSTD','#')
CALL MX3ALF('INSTR','&')
CALL MX4ALF('MATH','@')
CALL MX5ALF('SPEC','*')
CALL MX6ALF('L/CGREEK','!')
CALL SWISSL
CALL SHDCHR(90.,1.,.003,1)
CALL PAGE(11.0,8.5)
CALL NOBRDR
CALL HWR0T('COMIC')
CALL HWSCAL('SCREEN')
CALL XREVTK
CALL YREVTK
CALL AREA2D(8.0,6.0)

```

```

CALL HEIGHT(.2)
CALL YAXANG(0.0)
CALL XNAME('#T&E.7H.5%+&EXHX%',17)
CALL YNAME(' ',1)
X=-0.3
Y=5.00-.07
DY=1.00
CALL MESSAG('&H.7%O&HX%',10,X,Y)
CALL MESSAG('&H.7#NODE&A#3&HX%',17,4.8,4.45)
Y=Y-DY
CALL MESSAG('&H.7%1&HX%',10,X,Y)
CALL MESSAG('&P1A.2P2#U*,&A.2U1A-.2L.3U2B2L1.7%U&LX',
$38,-0.95,3.55)
CALL MESSAG('&H.7#NODE&A#1&HX%',17,4.8,2.45)
Y=Y-2.0*DY
CALL MESSAG('&H.7%1&HX%',10,X,Y)
CALL MESSAG('&H.7#NODE&A#2&HX%',17,4.8,0.45)
Y=Y-DY
CALL MESSAG('&H.7%O&HX%',10,X,Y)
CALL YINTAX
CALL XINTAX
CALL XTICKS(5)
CALL YTICKS(6)
CALL GRAF(0.0,5.0,XO(2),-1.0,1.0,1.0)
CALL FRAME
CALL CURVE(XO,YO,2,0)
CALL CURVE(XO,Y1,2,0)
CALL CURVE(XO,Y2,2,0)
CALL THKCRV(.02)
CALL CURVE(TIME,FYX,NDT,0)
CALL CURVE(TIME,FYY,NDT,0)
CALL CURVE(TIME,FYZ,NDT,0)
CALL ENDPL(0)
RETURN
END

```

```

*****
*          GENERAL INPUT          *
*****
*  SEED =      0.500             *
*  NTI  =      50                *
*  NP   =     1000               *
*  UT   =      3.142            *
*  HO   =      0.200            *
*  XSO  =     -1.000            *
*  HSO  =      2.000            *
*  USO  =      1.000            *
*  SIGX =      0.250            *
*  SIGY =      0.150            *
*  SIGZ =      0.150            *
*****

```

```

*****
*          NODAL INPUT           *
*****
*  NODE   THETA   R   H   UB   UW *
*    1     0.0000  1.0000  2.0000  1.0000  1.0000 *
*    2    180.0000  1.0000  2.0000  1.0000  1.0000 *
*****

```

```

*****
*          NORMALIZED TAU-SERIES          *
*****
*   SIGMAX= 0.9884 *   NORMALIZED VALUES *
*   SIGMAY= 0.9820 *           OF         *
*   SIGMAZ= 0.9922 *           SIGMA.     *
*****
*
*          - TAU-SERIES -
*
*   TAU      VX      VY      VZ      *
*   0.02     0.37332 -0.69509 -1.24651 *
*   0.04     0.63777 -0.72212 -1.56796 *
*   0.06     0.26754 -1.15913 -1.36602 *
*   0.08     0.10705 -0.58196 -1.29311 *
*   0.10     0.19798 -0.26178 -1.19314 *
*   0.12     0.29750  0.01191 -1.26982 *
*   0.14     0.41181 -0.04261 -1.45596 *
*   0.16     0.52025  0.01815 -1.38294 *
*   0.18     0.41273 -0.03464 -1.06189 *
*   0.20     0.60922  0.33550 -0.82090 *
*   0.22     0.38563 -0.26088 -1.03643 *
*   0.24     0.15804 -0.56701 -1.54245 *
*   0.26     0.17182 -0.63027 -1.29703 *
*   0.28     0.10774 -0.20067 -1.40332 *
*   0.30     0.15182 -0.73085 -1.55976 *
*   0.32     0.28635 -0.55088 -0.99271 *
*   0.34     0.08478  0.10643 -0.64033 *
*   0.36     -0.13336  0.13828 -0.44343 *
*   0.38     -0.08352  0.23518 -1.35516 *
*   0.40     0.06587  0.70043 -1.71169 *
*   0.42     0.10215  0.97482 -1.78938 *
*   0.44     0.09660  0.98281 -1.69888 *
*   0.46     -0.24217  0.95460 -1.65827 *
*   0.48     -0.64232  1.53277 -1.35484 *
*   0.50     -0.22485  1.36857 -1.08471 *
*   0.52     -0.01709  1.10538 -1.31461 *
*   0.54     -0.03725  1.33098 -1.48904 *
*   0.56     -0.12834  1.02669 -1.62649 *
*   0.58     -0.40085  1.38394 -1.71746 *
*   0.60     -0.34931  1.40100 -1.70282 *
*   0.62     -0.42870  0.70140 -1.40305 *
*   0.64     -0.67972  0.78570 -1.29736 *
*   0.66     -1.01550  1.34336 -1.16988 *
*   0.68     -1.03660  0.44165 -1.05963 *
*   0.70     -1.20016 -0.10771 -1.06437 *
*   0.72     -0.96281  0.37933 -1.20335 *
*   0.74     -1.01830  0.99451 -1.48014 *
*   0.76     -0.85504  1.52575 -1.22055 *
*   0.78     -0.94414  1.40130 -0.81961 *
*   0.80     -0.85580  1.87830 -0.98856 *
*****

```

```

*****
*   NODE      1          TIME-SERIES      *
*****
*   SIGMAU= 0.2458      *   SIMULATED VALUES      *
*   SIGMAV= 0.1502      *           OF           *
*   SIGMAW= 0.1511      *   SIGMA.           *
*****
*
*                   - TIME-SERIES -
*
*   TIME      THETA      U      V      W
*   0.04      7.20      0.11357  0.12456 -0.02814
*   0.08      14.40     0.15082  0.07614 -0.03858
*   0.12      21.60     0.14508  0.06319  0.03130
*   0.16      28.80     0.20446  0.01531 -0.11339
*   0.20      36.00     0.20824 -0.09096 -0.15517
*   0.24      43.20     0.14936 -0.15022 -0.10518
*   0.28      50.40     0.11071 -0.10533 -0.19965
*   0.32      57.60     0.02922 -0.08210 -0.19234
*   0.36      64.80     0.09211 -0.00329 -0.20780
*   0.40      72.00     0.10919 -0.00343 -0.17005
*   0.44      79.20     0.12116  0.00048 -0.14115
*   0.48      86.40     0.04232 -0.08279 -0.22762
*   0.52      93.60     0.04278 -0.09407 -0.19637
*   0.56     100.80     0.03403 -0.05864 -0.20344
*   0.60     108.00     0.03052 -0.04451 -0.20693
*   0.64     115.20     0.03301 -0.05455 -0.20445
*   0.68     122.40     0.04122 -0.08757 -0.19628
*   0.72     129.60     0.04042 -0.08755 -0.22169
*   0.76     136.80     0.08994 -0.04435 -0.16409
*   0.80     144.00     0.13730  0.03337 -0.13418
*   0.84     151.20     0.12888  0.00238 -0.20533
*   0.88     158.40     0.08018  0.00013 -0.19614
*   0.92     165.60     0.03170 -0.07686 -0.19071
*   0.96     172.80     0.14711 -0.11705 -0.23116
*   1.00     180.00     0.10086 -0.14398 -0.16835
*   1.04     187.20     0.15574 -0.14604 -0.10734
*   1.08     194.40     0.20849 -0.08201 -0.19131
*   1.12     201.60     0.21016 -0.07985 -0.15407
*   1.16     208.80     0.24383  0.03039 -0.13138
*   1.20     216.00     0.16442 -0.00496 -0.06721
*   1.24     223.20     0.18042 -0.00444  0.02586
*   1.28     230.40     0.18192  0.05262  0.03020
*   1.32     237.60     0.13362  0.06720  0.03475
*   1.36     244.80     0.14573  0.06719  0.04911
*   1.40     252.00     0.14941  0.06719  0.05347
*   1.44     259.20     0.14423  0.06719  0.04733
*   1.48     266.40     0.13447  0.06623  0.03161
*   1.52     273.60     0.19897  0.04454  0.02945
*   1.56     280.80     0.16451 -0.01218 -0.00680
*   1.60     288.00     0.21221  0.01828 -0.11693
*****

```

```

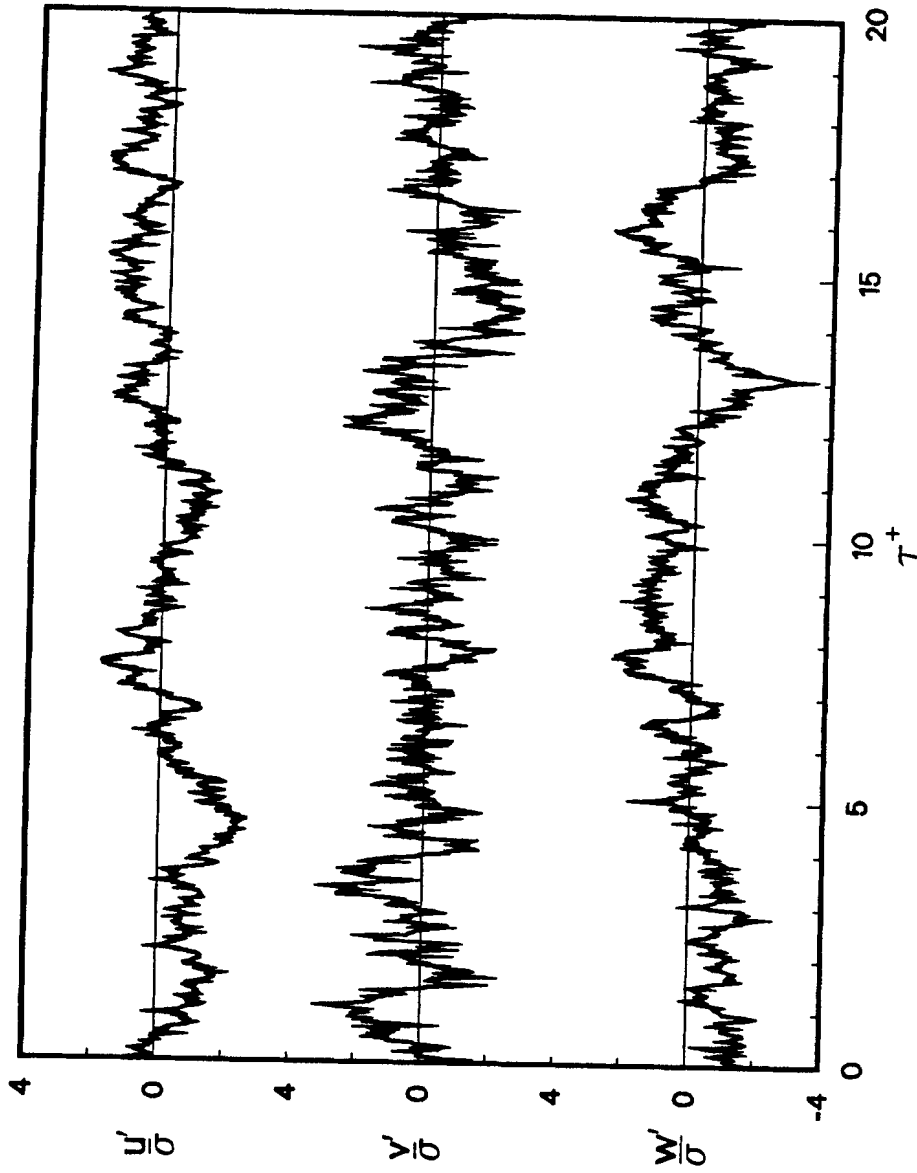
*****
*   NODE    2          TIME-SERIES
*****
*   SIGMAU= 0.2464    *   SIMULATED VALUES
*   SIGMAV= 0.1455    *           OF
*   SIGMAW= 0.1427    *           SIGMA.
*****
*
*           - TIME-SERIES -
*
*   TIME      THETA      U          V          W
*   0.04      187.20     0.21991  0.03037  -0.03176
*   0.08      194.40     0.21492  0.06500  0.06015
*   0.12      201.60     0.28584  0.23727  -0.00278
*   0.16      208.80     0.31905  0.25886  0.00536
*   0.20      216.00     0.26154  0.15101  -0.09355
*   0.24      223.20     0.27569  0.14645  -0.12770
*   0.28      230.40     0.22308  0.16625  -0.15416
*   0.32      237.60     0.19399  0.18274  -0.11729
*   0.36      244.80     0.20439  0.15600  -0.12203
*   0.40      252.00     0.20755  0.14788  -0.12348
*   0.44      259.20     0.20310  0.15931  -0.12145
*   0.48      266.40     0.19389  0.18691  -0.11882
*   0.52      273.60     0.23655  0.15770  -0.16544
*   0.56      280.80     0.26701  0.15067  -0.12029
*   0.60      288.00     0.29612  0.16421  -0.02885
*   0.64      295.20     0.28846  0.27682  -0.00346
*   0.68      302.40     0.21369  0.05464  0.06677
*   0.72      309.60     0.27637  0.04260  -0.05652
*   0.76      316.80     0.05629  0.06243  -0.04101
*   0.80      324.00     0.13773  0.11030  -0.02236
*   0.84      331.20     0.14529  -0.00960  -0.06586
*   0.88      338.40     0.18605  0.05144  0.03008
*   0.92      345.60     0.23635  0.02753  -0.12796
*   0.96      352.80     0.20844  -0.08121  -0.19527
*   1.00       0.00     0.10086  -0.14398  -0.16835
*   1.04       7.20     0.02979  -0.08089  -0.19197
*   1.08      14.40     0.12422  0.00100  -0.19698
*   1.12      21.60     0.04021  -0.08698  -0.22389
*   1.16      28.80     0.06938  -0.07831  -0.14659
*   1.20      36.00     0.00506  0.08375  -0.24042
*   1.24      43.20    -0.07191  0.15304  -0.24357
*   1.28      50.40    -0.00560  0.17470  -0.20407
*   1.32      57.60    -0.09882  0.20787  -0.25738
*   1.36      64.80    -0.14612  0.11306  -0.20062
*   1.40      72.00    -0.25797  0.09650  -0.16264
*   1.44      79.20    -0.26698  0.02454  -0.17127
*   1.48      86.40    -0.25389  0.14462  -0.21997
*   1.52      93.60    -0.21578  0.22492  -0.18501
*   1.56     100.80    -0.22617  0.21846  -0.14958
*   1.60     108.00    -0.23105  0.21437  -0.13639
*****

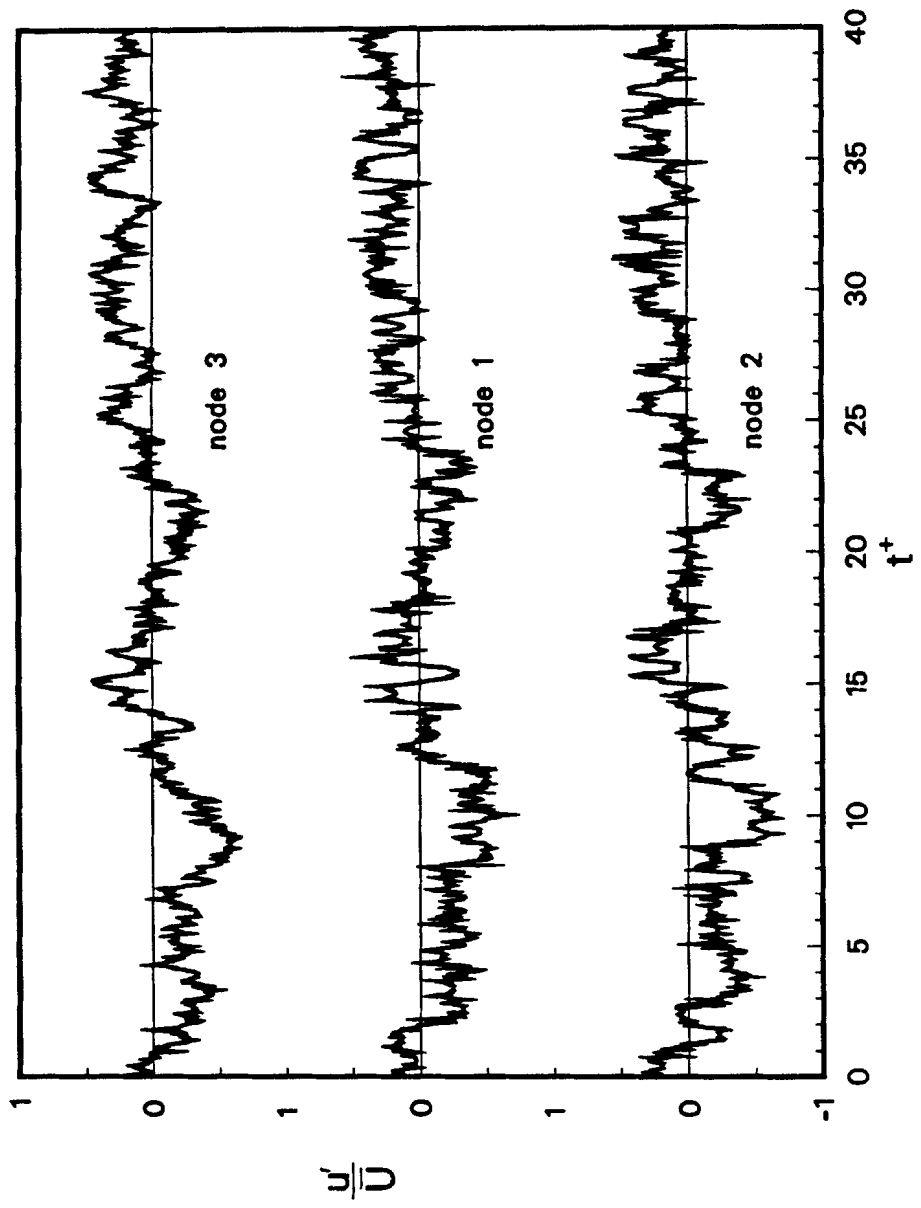
```

```

*****
*   NODE      3          TIME-SERIES          *
*****
*   SIGMAU= 0.2471    *   SIMULATED VALUES   *
*   SIGMAV= 0.1473    *           OF          *
*   SIGMAW= 0.1488    *           SIGMA.      *
*****
*
*                   - TIME-SERIES -
*
*   TIME      THETA      U          V          W
*   0.04      7.20      0.09333  -0.10426  -0.18698
*   0.08      14.40     0.15944  -0.10832  -0.23519
*   0.12      21.60     0.06689  -0.17387  -0.20490
*   0.16      28.80     0.02676  -0.08730  -0.19397
*   0.20      36.00     0.04949  -0.03927  -0.17897
*   0.24      43.20     0.07437   0.00179  -0.19047
*   0.28      50.40     0.10295  -0.00639  -0.21839
*   0.32      57.60     0.13006   0.00272  -0.20744
*   0.36      64.80     0.10318  -0.00520  -0.15929
*   0.40      72.00     0.15231   0.05032  -0.12314
*   0.44      79.20     0.09641  -0.03913  -0.15546
*   0.48      86.40     0.03951  -0.08505  -0.23137
*   0.52      93.60     0.04295  -0.09454  -0.19456
*   0.56     100.80     0.02694  -0.03010  -0.21050
*   0.60     108.00     0.03795  -0.10963  -0.23396
*   0.64     115.20     0.07159  -0.08263  -0.14891
*   0.68     122.40     0.02120   0.01596  -0.09605
*   0.72     129.60    -0.03334   0.02074  -0.06652
*   0.76     136.80    -0.02088   0.03528  -0.20327
*   0.80     144.00     0.01646   0.10506  -0.25675
*   0.84     151.20     0.02554   0.14622  -0.26841
*   0.88     158.40     0.02415   0.14742  -0.25483
*   0.92     165.60    -0.06054   0.14319  -0.24874
*   0.96     172.80    -0.16057   0.22991  -0.20323
*   1.00     180.00    -0.05622   0.20529  -0.16271
*   1.04     187.20    -0.00428   0.16581  -0.19719
*   1.08     194.40    -0.00931   0.19964  -0.22335
*   1.12     201.60    -0.03208   0.15401  -0.24397
*   1.16     208.80    -0.10021   0.20759  -0.25762
*   1.20     216.00    -0.08733   0.21015  -0.25542
*   1.24     223.20    -0.10717   0.10522  -0.21046
*   1.28     230.40    -0.16993   0.11785  -0.19461
*   1.32     237.60    -0.25387   0.20150  -0.17548
*   1.36     244.80    -0.25915   0.06626  -0.15895
*   1.40     252.00    -0.30004  -0.01615  -0.15966
*   1.44     259.20    -0.24071   0.05689  -0.18050
*   1.48     266.40    -0.25457   0.14917  -0.22202
*   1.52     273.60    -0.21376   0.22886  -0.18309
*   1.56     280.80    -0.23603   0.21020  -0.12295
*   1.60     288.00    -0.21395   0.28174  -0.14828
*****

```





(This page intentionally left blank)

DISTRIBUTION

Alcoa Technical center (5)
Aluminum Company of America
Alcoa Center, PA 15069
Attn: D. K. Ai
J. T. Huang
J. R. Jombock
M. Klingensmith
J. L. Prohaska

Alternative Sources of Energy
Milaca, MN 56353
Attn: L. Stoiaken

Amarillo College
Amarillo, TX 79100
Attn: E. Gilmore

American Wind Energy Association
1516 King Street
Alexandria, VA 22314

Arizona State University
University Library
Tempe, AZ 85281
Attn: M. E. Beecher

Dr. A. S. Barker
Trinity Western
7600 Glover Road
Langley, BC
CANADA V3A 4R9

Battelle-Pacific Northwest Laboratory
PO Box 999
Richland, WA 99352
Attn: L. Wendell

Bechtel Group, Inc.
PO Box 3965
San Francisco, CA 94119
Attn: B. Lessley

Dr. George Bergeles
Dept. of Mechanical Engineering
National Technical University
42, Patission Street
Athens, GREECE

Bonneville Power Administration
PO Box 3621
Portland, OR 97208
Attn: N. Butler

Burns and Roe, Inc.
800 Kinderkamack Road
Oradell, NJ 07649
Attn: G. A. Fontana

Canadian Standards Association
178 Rexdale Blvd.
Rexdale, Ontario, M9W 1R3
CANADA
Attn: T. Watson

Mark Chappel
Division of Energy
National Research Council
of Canada
Montreal Road
Ottawa, Ontario
CANADA K1A 0R6

Professor V. A. L. Chasteau
School of Engineering
University of Auckland
Private Bag
Auckland, NEW ZEALAND

Colorado State University
Dept. of Civil Engineering
Fort Collins, CO 80521
Attn: R. N. Meroney

Commonwealth Electric Co.
Box 368
Vineyard Haven, MA 02568
Attn: D. W. Dunham

Gale B. Curtis
Curtis Associates
3089 Oro Blanco Drive
Colorado Springs, CO 80917

M. M. Curvin
11169 Loop Road
Soddy Daisy, TN 37379

Department of Economic Planning
and Development
Barrett Building
Cheyenne, WY 82002
Attn: G. N. Monsson

Otto de Vries
National Aerospace Laboratory
Anthony Fokkerweg 2
Amsterdam 1017
THE NETHERLANDS

DOE/ALO
Albuquerque, NM 87115
Attn: G. P. Tennyson

DOE/ALO
Energy Technology Liaison Office
NGD
Albuquerque, NM 87115
Attn: Capt. J. L. Hanson, USAF

DOE Headquarters (20)
Wind/Oceans Technologies Division
1000 Independence Avenue
Washington, DC 20585
Attn: D. F. Ancona
P. R. Goldman

J. B. Dragt
Nederlands Energy Research Foundation
(E.C.N.)
Physics Department
Westerduinweg 3 Petten (nh)
THE NETHERLANDS

Dynergy Systems Corporation
821 West L Street
Los Banos, CA 93635
Attn: C. Fagundes

Dr. Norman E. Farb
10705 Providence Drive
Villa Park, CA 92667

Electric Power Research Institute
3412 Hillview Avenue
Palo Alto, CA 94304
Attn: E. Demeo
F. Goodman

Alcir de Faro Orlando
Pontificia Universidade Catolica-PUC/Rj
Mechanical Engineering Department
R. Marques de S. Vicente 225
Rio de Janeiro, BRAZIL

A. D. Garrad
Garrad Hasson
10 Northampton Square
London EC1M 5PA
UNITED KINGDOM

Gates Learjet
Mid-Continent Airport
PO Box 7707
Wichita, KS 67277
Attn: G. D. Park

H. Gerardin
Mechanical Engineering Department
Faculty of Sciences and Engineering
Universite Laval-Quebec, G1K 7P4
CANADA

R. T. Griffiths
University College of Swansea
Dept. of Mechanical Engineering
Singleton Park
Swansea, SA2 8PP
UNITED KINGDOM

Helion, Inc.
Box 445
Brownsville, CA 95919
Attn: J. Park, President

FloWind Corporation (3)
1183 Quarry Lane
Pleasanton, CA 94566
Attn: L. Schienbein
I. Vas
B. Im

Indal Technologies, Inc. (2)
3570 Hawkestone Road
Mississauga, Ontario
CANADA L5C 2V8
Attn: D. Malcolm
C. Wood

Institut de Recherche d'Hydro-Quebec
1800, Montee Ste-Julie
Varenes, Quebec, JOL 2P0
CANADA
Attn: Gaston Beaulieu
Bernard Masse

Iowa State University
Agricultural Engineering, Room 213
Ames, IA 50010
Attn: L. H. Soderholm

K. Jackson
West Wind Industries
P.O. Box 1705
Davis, CA 95617

M. Jackson
McAllester Financial
1816 Summit
W. Lafayette, IN 47906

Kaiser Aluminum and Chemical
Sales, Inc.
14200 Cottage Grove Avenue
Dolton, IL 60419
Attn: A. A. Hagman

Kaiser Aluminum and Chemical
Sales, Inc.
6177 Sunol Blvd.
PO Box 877
Pleasanton, CA 94566
Attn: D. D. Doerr

Kansas State University
Electrical Engineering Department
Manhattan, KS 66506
Attn: Dr. G. L. Johnson

R. E. Kelland
The College of Trades and Technology
PO Box 1693
Prince Philip Drive
St. John's, Newfoundland, A1C 5P7
CANADA

KW Control Systems, Inc.
RD No.4, Box 914C
South Plank Road
Middletown, NY 10940
Attn: R. H. Klein

Kalman Nagy Lehoczky
Cort Adelaers GT. 30
Oslo 2, NORWAY

L. K. Liljergre
1260 S.E. Walnut No.5
Tustin, CA 92680

L. Liljidahl
Building 005, Room 304
Barc-West
Beltsville, MD 20705

Olle Ljungstrom
FFA, The Aeronautical Research
Institute
Box 11021
S-16111 Bromma, SWEDEN

Robert Lynette
R. Lynette and Assoc., Inc.
15921 SE 46th Way
Bellevue, WA 98006

Massachusetts Institute of Technology
77 Massachusetts Avenue
Cambridge, MA 02139
Attn: Professor N. D. Ham
W. L. Harris, Aero/Astro Dept.

H. S. Matsuda
Composite Materials Laboratory
Pioneering R and D Laboratories
Toray Industries, Inc.
Sonoyama, Otsu, Shiga, JAPAN 520

G. M. McNerney
US Wind Power
160 Wheeler Road
Burlington, MA 01803

Michigan State University
Division of Engineering Research
East Lansing, MI 48825
Attn: O. Krauss

Napier College of Commerce and
Technology
Tutor Librarian, Technology Faculty
Colinton Road
Edinburgh, EH10 5DT
ENGLAND

National Rural Electric
Cooperative Assn
1800 Massachusetts Avenue NW
Washington, DC 20036
Attn: Wilson Prichett, III

Natural Power, Inc.
New Boston, NH 03070
Attn: Leander Nichols

Northwestern University
Dept. of Civil Engineering
Evanston, IL 60201
Attn: R. A. Parmalee

Ohio State University
Aeronautical and Astronautical Dept.
2070 Neil Avenue
Columbus, OH 43210
Attn: Professor G. Gregorek

Oklahoma State University
Mechanical Engineering Dept.
Stillwater, OK 76074
Attn: D. K. McLaughlin

Oregon State University
Mechanical Engineering Dept.
Corvallis, OR 97331
Attn: R. E. Wilson

Pacific Gas and Electric
3400 Crow Canyon Road
San Ramon, CA 94583
Attn: T. Hillesland

Ion Paraschivoiu
Department of Mechanical Engineering
Ecole Polytechnique
CP 6079
Succursale A
Montreal H3C 3A7
CANADA

Riso National Laboratory
Postbox 49
DK-4000 Roskilde
DENMARK
Attn: Troels Friis Pedersen
Helge Petersen

Jacques Plante
Hydro Quebec
Place Dupuis Ile etage
855 est rue Ste-Catherine
Montreal, Quebec
CANADA H2L 4P5

The Power Company, Inc.
PO Box 221
Genesee Depot, WI 53217
Attn: A. A. Nedd

Power Technologies Inc.
PO Box 1058
Schenectady, NY 12301-1058
Attn: Eric N. Hinrichsen

Public Service Co. of New Hampshire
1000 Elm Street
Manchester, NH 03105
Attn: D. L. C. Frederick

Public Service Company of New Mexico
PO Box 2267
Albuquerque, NM 87103
Attn: M. Lechner

RANN, Inc.
260 Sheridan Ave., Suite 414
Palo Alto, CA 94306
Attn: A. J. Eggers, Jr.

The Resources Agency
Department of Water Resources
Energy Division
PO Box 388
Sacramento, CA 95802
Attn: R. G. Ferreira

Dr. R. Ganesh Rajagopalan, Asst. Prof.
Aerospace Engineering Department
Iowa State University
404 Town Engineering Bldg.
Ames, IA 50011

Reynolds Metals Company
Mill Products Division
6601 West Broad Street
Richmond, VA 23261
Attn: G. E. Lennox

R. G. Richards
Atlantic Wind Test Site
PO Box 189
Tignish P.E.I., COB 2B0
CANADA

A. Robb
Memorial University of Newfoundland
Faculty of Engineering and Applied
Sciences
St. John's Newfoundland, A1C 5S7
CANADA

Solar Energy Research Institute
1617 Cole Boulevard
Golden, CO 80401
Attn: R. W. Thresher

Dr. Ing. Hans Ruscheweyh
Institut fur Leichbau
Technische Hochschule Aachen
Wullnerstrasse 7
FEDERAL REPUBLIC OF GERMANY

Beatrice de Saint Louvent
Etablissement d'Etudes et de
Recherches
Meteorologigues
77 Rue de Servas
92106 Boulogne-Billancourt Cedex
FRANCE

Gwen Schreiner
Librarian
National Atomic Museum
Albuquerque, NM 87185

Arnan Seginer
Professor of Aerodynamics
Technion-Israel Institute of Technology
Department of Aeronautical Engineering
Haifa
ISRAEL

Mr. Farrell Smith Seiler, Editor
Wind Energy Abstracts
PO Box 3870
Bozeman, MT 59772-3870

David Sharpe
Dept. of Aeronautical Engineering
Queen Mary College
Mile End Road
London, E1 4NS
UNITED KINGDOM

Kent Smith
Instituto Tecnológico Costa Rico
Apartado 159 Cartago
COSTA RICA

Bent Sorenson
Roskilde University Center
Energy Group, Bldg. 17.2
IMFUFA
PO Box 260
DK-400 Roskilde
DENMARK

Peter South
ADECON
32 Rivalda Road
Weston, Ontario, M9M 2M3
CANADA

Southern California Edison
Research and Development Dept., Room 497
PO Box 800
Rosemead, CA 91770
Attn: R. L. Scheffler

G. Stacey
The University of Reading
Department of Engineering
Whiteknights, Reading, RG6 2AY
ENGLAND

Stanford University
Dept. of Aeronautics and
Astronautics Mechanical Engineering
Stanford, CA 94305
Attn: Holt Ashley

Dr. Derek Taylor
Alternative Energy Group
Walton Hall
Open University
Milton Keynes, MK7 6AA
UNITED KINGDOM

R. J. Templin (3)
Low Speed Aerodynamics Laboratory
NRC-National Aeronautical Establishment
Montreal Road
Ottawa, Ontario, K1A 0R6
CANADA

Texas Tech University (2)
Mechanical Engineering Dept.
PO Box 4289
Lubbock, TX 79409
Attn: J. W. Oler

K. J. Touryan
Moriah Research
6200 Plateau Dr.
Englewood, CO 80111

Tulane University
Dept. of Mechanical Engineering
New Orleans, LA 70018
Attn: R. G. Watts

Tumac Industries, Inc.
650 Ford Street
Colorado Springs, CO 80915
Attn: J. R. McConnell

J. M. Turner
Terrestrial Energy Technology
Program Office
Energy Conversion Branch
Aerospace Power Division/
Aero Propulsion Lab
Air Force Systems Command (AFSC)
Wright-Patterson AFB, OH 45433

United Engineers and Constructors, Inc.
PO Box 8223
Philadelphia, PA 19101
Attn: A. J. Karalis

Universal Data Systems
5000 Bradford Drive
Huntsville, AL 35805
ATTN: C. W. Dodd

University of California
Institute of Geophysics
and Planetary Physics
Riverside, CA 92521
Attn: Dr. P. J. Baum

University of Colorado
Dept. of Aerospace Engineering Sciences
Boulder, CO 80309
Attn: J. D. Fock, Jr.

University of Massachusetts
Mechanical and Aerospace
Engineering Dept.
Amherst, MA 01003
Attn: Dr. D. E. Cromack

University of New Mexico
New Mexico Engineering
Research Institute
Campus P.O. Box 25
Albuquerque, NM 87131
Attn: G. G. Leigh

University of Oklahoma
Aero Engineering Department
Norman, OK 73069
Attn: K. Bergey

University of Sherbrooke
Faculty of Applied Science
Sherbrooke, Quebec, J1K 2R1
CANADA
Attn: A. Laneville
P. Vittecoq

The University of Tennessee
Dept. of Electrical Engineering
Knoxville, TN 37916
Attn: T. W. Reddoch

USDA, Agricultural Research Service
Southwest Great Plains Research Center
Bushland, TX 79012
Attn: Dr. R. N. Clark

Utah Power and Light Co.
51 East Main Street
PO Box 277
American Fork, UT 84003
Attn: K. R. Rasmussen

Dirk Vandenberghe
State Univ. of Ghent
St. Pietersnieuwstraat 41
9000 Ghent
BELGIUM

W. A. Vachon
W. A. Vachon and Associates
PO Box 149
Manchester, MA 01944

VAWTPOWER, Inc.
134 Rio Rancho Drive
Rio Rancho, NM 87124
Attn: P. N. Vosburgh

Washington State University
Dept. of Electrical Engineering
Pullman, WA 99163
Attn: F. K. Bechtel

West Texas State University
Government Depository Library
Number 613
Canyon, TX 79015

West Texas State University
Department of Physics
P.O. Box 248
Canyon, TX 79016

West Virginia University
Dept. of Aero Engineering
1062 Kountz Avenue
Morgantown, WV 26505
Attn: R. Walters

D. Westlind
Central Lincoln People's Utility
District
2129 North Coast Highway
Newport, OR 97365-1795

Wichita State University
Aero Engineering Department (2)
Wichita, KS 67208
Attn: M. Snyder
W. Wentz

Wind Power Digest
PO Box 700
Bascom, OH 44809
Attn: Michael Evans

Wisconsin Division of State Energy
8th Floor
101 South Webster Street
Madison, WI 53702
Attn: Wind Program Manager

1000 W. F. Brinkman
1510 J. W. Nunziato
1520 W. Hermann(actg)
1522 R. C. Reuter, Jr.
1523 J. H. Biffle
1524 A. K. Miller
1530 L. W. Davison
1540 W. C. Luth
1550 R. C. Maydew
1551 J. K. Cole
1552 C. W. Peterson
1552 J. H. Strickland (25)
1553 S. McAlees, Jr.
1554 D. D. McBride
1555 W. R. Barton
1556 W. L. Oberkampf
1556 G. F. Homicz
2525 R. P. Clark
3142 S. A. Landenberger (5)
3151 W. L. Garner (3)
3154-3 C. H. Dalin (28)
For DOE/OSTI (Unlimited
Release)

3160 J. E. Mitchell (15)
3161 P. S. Wilson
6000 D. L. Hartley
6200 V. L. Dugan
6225 H. M. Dodd (50)
6225 T. D. Ashwill
6225 D. E. Berg
6225 L. R. Gallo
6225 P. C. Klimas
6225 D. S. Oscar
6225 M. E. Ralph
6225 D. C. Reda
6225 M. A. Rumsey
6225 W. A. Stephenson
6225 H. J. Sutherland
7111 J. W. Reed
7544 D. R. Schafer
7544 T. G. Carne
7544 J. Lauffer
8024 P. W. Dean
9100 R. G. Clem
9122 T. M. Leonard